Title

Cooperative roles of Hras and Kras in controlling inflammation during tumor evolution

Permalink

https://escholarship.org/uc/item/2288x0c7

Author

Bollam, Saumya Reddy

Publication Date

2024

Peer reviewed|Thesis/dissertation

Cooperative roles of Hras and Kras in controlling inflammation during tumor evolution

by
Saumya Reddy Bollam

DISSERTATION
Submitted in partial satisfaction of the requirements for degree of
DOCTOR OF PHILOSOPHY

in

Biomedical Sciences

in the

GRADUATE DIVISION
of the
UNIVERSITY OF CALIFORNIA, SAN FRANCISCO

Approved:

Tiffany Scharschmidt
_____
Chair

Allan Balmain
Allan Balmain
_____
Rohit Bose
Rohit Bose
_____
Michael Oldham
Michael Oldham
_____

_____
Committee Members

Dedication

To my teachers, for instilling in me a stubborn curiosity only addressable by undertaking a PhD;

To my friends, for believing I could excel at my work and do something important;

To my family, for holding every other part of my life together so I could focus on this task.

Acknowledgements

I am indebted to many people who supported me throughout this project and got me here. Primarily, to my PI, Allan Balmain, who accepted an email from a first year graduate student with no experience in skin biology and an interest in learning new computational methods for studying cancer biology. Allan is a kind and thoughtful scientist, respected by every single one of his peers. It is hard to overstate how much I have gained because Allan's colleagues' trust in his decisions extends to their trust in me. Every opportunity and success I have celebrated over the past 5 years is because I have been able to stand on his shoulders. I hope to one day pay forward this debt, and also lead a group with his measured confidence.

Two groups of UCSF professors evaluated and assessed my progress. For my qualifying exam, Rohit Bose, Marina Sirota, Mary Helen Barcellos-Hoff, and Russ Pieper generously accepted my ask for guidance during the summer of 2020, when the pandemic was still terrifying, fires were raging, and nobody had extra energy to offer anyone else. That this group showed up for me despite the innumerable personal challenges they faced during this time is a gift I do not take lightly. Over the course of my thesis work, Tiffany Scharschmidt, Rohit Bose, Michael Oldham, and Allan Balmain served as my thesis committee. This group offered me much needed encouragement and affirmations, and challenged me to meet a standard I did not know I could hold myself to. Thank you for believing in me and this science.

The basis of the work presented here was produced over a number of years by many past members of the Balmain Lab. I am particularly indebted to the efforts of Reyno Del Rosario and Di Wu, without whom my studies would still be ongoing. Without Andrea Curtabbi and Aaron Huebner, my ideas would still be in my own head. Thank you for giving me the space to think out

loud and being patient soundboards for everything from my wacky to my logical ideas. Without Eve Kandyba, Giovanna Nappo, Anna Hakes, and Diana Cristea, I could not have survived being a graduate student during COVID. Thank you to my council of sanity.

I also want to say thank you to a few important groups of people:

To my classmates, for letting me learn and grow beside you;

To my coworkers and labmates, for celebrating the wins and lifting me up after setbacks;

To my first lab environments, for taking a chance on me;

To my students, for also taking a chance on learning with me; and,

this project would have been utterly impossible without the emotional, spiritual, scientific, moral, financial, unconditional, and/or inadvertent support offered by those in the following, regrettably inexhaustive, list:

Steven Adler, Michael Adler, Alexandra Amen, Bruce and Liz Ashley, Madison Ashley, Siddhartha Basu, Joni Borbon, Katie Bui, Matt Chan, Neal Chaudhuri, Sudha Cheemakurthi, Neeraj Chinthireddi, Sara Chiu, Tom Christiansen, Cherie Chung, Caroline Cotto, VP Dao, Francoise Dastous, Rhogerry Deschyka, Kaitlin Dickson, Julie and Noel Garcia, Michelle Goldberg, Beenu Govindrao, Anna Hakes, Stephanie Hilz, Alex Hilleary, David Horowitz, Alison Hu, Sona Jain, Trishla Jain, Hari Kandadai, Andrae Ladores, Michael Liu, Nicholas Hsin-Ping Maffei Lee, Marissa Mason, Radhika Mathur, Tanushri and Nishith Mathur, Bradon McDonald, Andrew McKinney, Aidan McLeod, Michael Meaney, Michael Mobaraki, Birgit Musheno, Giovanna Nappo, Zun Zar Chi Naing, Neha Parvathala, Praveen Parvathala, Rajeev Parvathala, Shobha Parvathala, Kavitha Perumparaichallai, Patricia and Nicole Petersen, Darshana Prakasam, Sampath Rangasamy, Carolyn Rath, Rebecca Rinehart, Nicholas Stevers, Daphne Superville, Alex Theos, Susan Tu, Priya Varra, Ram Varra, Shreya Varra, Vamsi Varra, Sonia Vora, Alicia Wun, Ted Wun, Chunling Yi, Amy Young, Carlos Zuazo

Contributions

The work in this thesis represents my independent writing, with critical guidance from my advisor, Allan Balmain, and my committee, Tiffany Scharschmidt, Rohit Bose, and Michael Oldham. The findings are being prepared for publication as follows:

Chapter 2 forms the basis of a manuscript in which the co-authors Reyno del Rosario and Allan Balmain will be included for their contributions to mouse experiments, funding acquisition, and overall direction.

Chapter 3 forms the basis of a manuscript in which the co-authors Di Wu, Chris Hsiung, Diana Cristea, Reyno Del Rosario, Charles Voliva, Luke Gilbert, Rosemary Akhurst, and Allan Balmain will be included for their contributions to experimental design, materials and funding acquisition, cell line construction, mouse experiments, and overall direction.

Cooperative roles of *Hras* and *Kras* in controlling inflammation during tumor evolution

Saumya Reddy Bollam

Abstract

Although chronic inflammation promotes cancer development, an unresolved paradox is how tumors become proficient at evading the immune system. To achieve this, tumor oncogenes must both cooperate with inflammatory signals to promote tumorigenesis and drive immune evasion. In this study, we use gene expression networks to demonstrate the cooperative roles of two of the most frequently mutated oncogenes, *Hras* and *Kras*, in controlling inflammation during cutaneous squamous cell carcinoma (cSCC) development. First, we describe the role of *Hras* in orchestrating the tissue response to 12-O-tetradecanoylphorbol acetate (TPA), a tumor promoter used in the chemical carcinogenesis model of cSCC. In this model, *Hras* is necessary for TPA-induced promotion, as germline loss of *Hras* reduces tumorigenesis. We find that the TPA response induces recruitment of regulatory T cells in an *Hras*-dependent manner. We further demonstrate that the loss of *Hras* also leads to an increase in activated dendritic cells and neutrophils during the TPA response. These findings suggest that *Hras* may be necessary for neoplastic cells to survive TPA-induced inflammation. Second, we explored the role of *Kras* in evading anti-tumor immunity. In a pooled *in vivo* CRISPRi screen, we tested the hypothesis that genes strongly co-expressed with mutant *Kras* might mediate resistance to immune checkpoint blockade therapy with anti-PD1. From this screen, we identified 2 targets, *Sgol2* and *Rc3h2*, which when knocked down successfully resensitized *Kras* mutant cSCCs to treatment with anti-PD1. Collectively, this supports the conclusion that *Hras* and *Kras* play fundamental, but distinct roles in adapting to inflammation at different stages of cSCC development.

Table of Contents

List of Figures

List of Abbreviations

aPD1 (anti - programmed death ligand 1)

CRISPRi (clustered interspaced short palindromic repeats, inactivation)

cSCC (cutaneous squamous cell carcinoma)

d9K (dead-Cas9-KRAB domain)

DMBA (7,12-Dimethylbenzanthracene)

Hras/*HRAS* (Harvey Rat Sarcoma viral oncogene)

ICI (immune checkpoint inhibitor)

IP (intraperitoneal)

Kras/*KRAS* (Kirsten Rat Sarcoma viral oncogene)

KO (knock out)

PD1 (programmed death ligand 1)

RNAseq (RNA sequencing, refers to 3' bulk RNA sequencing)

sgRNA (single guide RNA)

sgNT1 (single guide non targeting sequence 1)

TPA (12-O-tetradecanoylphorbol-13-acetate)

TRG (TPA responsive genes)

WT (wild type)

Chapter 1: Introduction

Chronic inflammation and oncogenesis

Chronic inflammation is associated with cancer risk across almost every cancer-prone tissue[1,2]. Depending on the tissue, inflammation can be the result of anything from physical tissue damage to chemical environmental stress. In each of these circumstances, there is a careful balance between recruiting immune cells that recognize and clear damaged cells and subsequently regulating these immune cells to restore healthy homeostasis. Importantly, when these tissue intrinsic repair processes are disrupted, tumorigenesis can be promoted.

In many ways, the gradual development of a tumor itself constitutes a significant tissue injury which prompts immune surveillance. Tumor evolution begins with a neoplastic cell that carries an oncogenic mutation, and culminates in the growth of an invasive mass that can often metastasize to distant tissues. During each of these stages, the tissue sustains both molecular and physical injuries that can trigger immunological involvement. Therefore, to successfully transform into a malignant tumor, a neoplastic cell and its progeny must be able to continuously escape a highly-evolved set of defenses designed to detect and eliminate such threats to the body.

Initially, cells which have accumulated significant amounts of DNA damage and oncogenic mutations must escape immune detection and clearance. Indeed, it has been shown in normal healthy-appearing tissue from donors who died of non-health related causes that there are significant populations of cells which carry oncogenic mutations without causing pathological symptoms[3,4]. How do these cells manage to evade detection and elimination for so many years? Is it possible that the initiating mutation confers some of these immune evasion phenotypes? The study of the mechanisms that protect these cells from elimination is an active area of research,

along with the mechanisms that induce, or "promote", their growth. Transformed cells, and cell populations, which sit indolently while harboring oncogenic mutations have the potential to undergo promotion -- a non-mutagenic stage of tumorigenesis leading to neoplasms. Models of promoters used in mouse *in vivo* studies include chemical irritants which reproduce an inflammatory environment that eventually results in neoplastic growth. However, it is yet to be fully understood how the initiated cell and surrounding healthy tissue respond to promoters which cause inflammatory injury.

Additionally, tumor masses that have become invasive and compromise healthy tissue functions must also attenuate or escape the consequences of the wound repair mechanisms they have initiated. In the skin, for example, wound healing involves inflammation, new tissue growth, and re-epithelialization. Damaged cells are cleared away by macrophages, the tissue must be re-vascularized, and then remodeled – each of these steps presents a threat of detection and elimination to neoplastic cells. Any oncogenic mutations which provide a selective advantage in those environments to survive will therefore be present in the resulting tumor. Tumors use multiple strategies to achieve this, including hijacking the signals which are produced during inflammation, redirecting new vascularization to itself, and importantly evasion of detection by cytotoxic T cells. Understanding how activated oncogenes lead to these outcomes is thus an important focus of active research.

Ras driven oncogenesis

Across all human cancers, over 30% are driven by activating mutations in the Ras genes: *Kras*, *Hras*, and Nras. Each of these genes encodes a GTPase most often found at the plasma membrane as a signal transducer for a variety of functions encompassing cell proliferation, survival, and differentiation. Their sequences are highly conserved, with variation found only at the C-terminal hypervariable region. Due to the high level of sequence conservation across the

regions responsible for downstream effector signaling, the literature suggests that *Hras* and *Kras* have similar functions in the different cells they are expressed in. However, most post-translational modifications are found in the hypervariable region, which implies that there may be RAS homolog specific functions which are underappreciated as yet.

Oncogenic mutations across all three Ras genes most commonly occur at hotspot codons G12, G13, and Q61, rendering the protein locked in its active, GTP-bound state. These gain-of-function mutations lead to constitutive activation of downstream effector signaling like the MAPK/ERK and PI3K/AKT pathways. With these pathways hyperactivated, cell proliferation can thus proceed unrestricted and lead to tumorigenesis. Interestingly, over the past few decades there have been reports of mutation-specific consequences, demonstrating not only different effects of a G12 mutation compared to a Q61 mutation, but also different effects of a G12D mutation compared to G12C[5]. Within the spectrum of *Kras* mutations alone, the relative prevalence of each is also highly specific to the tissue of origin. For example, in human lung adenocarcinoma (LUAD), the most common *Kras* driver mutation is G12C, in human pancreatic ductal adenocarcinoma (PDAC) it is G12D, and G13D is most commonly found human colorectal cancers (CRC). This incredible tissue specificity of mutation prevalence is an active area of research which has wide-reaching implications for development of effective treatments.

Furthermore, there is remarkable tropism in which Ras genes are associated with specific cancers. Activating mutations in *Kras* are selectively found in lung, pancreas, and colorectal cancers while those in *Hras* are selectively found in head and neck squamous cell carcinoma (HNSCC) and bladder cancers; melanomas, leukemias, and myelomas are most commonly driven by oncogenic Nras mutations. It is extremely rare to find counterexamples to these patterns and the reasons behind this specificity are unresolved. These observations then necessarily beg the question of what distinct functions *Kras*, *Hras*, and Nras are orchestrating.

Decades of research on the functions of these activated Ras proteins across human cancers has demonstrated the activated and acquired consequences of these mutations within the cell. The massive web of Ras signaling pathways activated by each specific mutation, within cells from specific tissues, has been studied and validated across most models used in biological research. Thus, one way to understand the specific roles of the different Ras homologs is to compare the acquired functions of oncogenic mutations in each of these genes. This comparison of oncogenic *Kras* with oncogenic *Hras* demonstrated differential strength in activating multiple downstream effectors and decision to trigger apoptosis[6,7]. For example, *Kras* G12V was shown to have increased ability to activate Rac, in comparison with *Hras* G12V[7]. While these studies demonstrate the role of activated Ras in tumor formation, they often overlook the potential role of the WT allele during homeostasis.

In the early phases of tumorigenesis, the initiated tumor cell can carry just a single activating mutation. In these cells, the wild-type allele is still intact and can contribute contradictory signaling to the mutant allele. Here, we introduce another important question regarding the differential roles of wildtype Ras with mutant Ras. It became clear that the wildtype Ras allele is a hindrance to tumorigenesis with increasing reports of allelic imbalances in mutant Ras driven cancers [8,9]. Often, the wild-type Ras allele is ultimately lost in the tumor, or there is amplification of the mutant Ras allele. The mechanisms underlying dependence on increased mutant Ras signaling may also be Ras homolog specific, as different mechanisms have been reported in the context of *Kras* and Nras [10,11]. Thus, a survey of Ras specific activity of wildtype and mutant alleles is an important unmet need in cancer biology.

Chemical carcinogenesis model of cutaneous squamous cell carcinoma (cSCC)

In order to understand the differential roles of Ras in tumorigenesis, we use a model of chemically induced cSCC, where tumor development relies on two steps – initiation and

promotion. Initiation is the process by which mutations are induced in the tissue. DMBA, or 7,12-Dimethylbenzanthracene, induces A:T mutations across the genome and can initiate the full repertoire of oncogenic Ras mutations in the skin. However, following promotion by TPA, or 12-O-Tetradecanoylphorbol-13-acetate, there is a robust selection for *Hras*Q61L mutant cSCCs. Promoting agents like TPA do not themselves induce further mutations and are not associated with a specific mutation signature, and yet they are necessary to induce tumors. In comparison to genetic models, commonly induced by a tissue specific Cre which drives the overexpression of a mutant allele in every cell of a tissue, chemically induced models more accurately recapitulate the tissue environment experienced by tumor initiating cells since it sets up a system where there are a few mutant cells competing with normal healthy cells[12].

In this model, wildtype FVB mice reliably produce *Hras*Q61L mutant cSCCs in response to carcinogenesis with DMBA and TPA. In *Hras*^{-/-} mice, DMBA and TPA instead promotes *Kras*[MUT] cSCCs [2,13]. Therefore, this model presents a novel opportunity to address differences in wildtype and mutant Ras signaling between two Ras homologs in the same cancer type. In the absence of confounding features of tissue origin difference, we can begin to disentangle the distinct functions addressed by *Hras* and *Kras*, whether it is wildtype or mutant, during tumor promotion and malignant progression. Skin carcinogenesis thus presents an apt model for the studies detailed in this work, because of the ability to visually assess progression through tumor evolution.

As an interesting note, cutaneous squamous cell carcinoma in humans is epidemiologically associated to HPV, and its incidence is associated with immunosuppressive states like those seen in organ transplantation. However, it is not clear why viral infection or reduced immunity leads to tumor progression[14]. One hypothesis suggests that HPV induces an immunosuppressed state, similar to that induced in organ transplant recipients, which allows for

transformed cells to escape immune clearance and progress into SCC. Thus, it would be advantageous to understand how cSCC innately coordinates its evasion of the immune system.

Rationale of study

With this immense body of literature in mind, the study described across the next two chapters attempts to describe the specific roles of *Hras* and *Kras* in tumor evolution. A preliminary analysis of cSCCs driven by oncogenic mutations in either *Hras* or *Kras* revealed distinct gene expression programs correlated with the driving oncogene. This laid the foundation for addressing two major goals. First, to establish how *Hras* allows normal keratinocytes to coordinate with tumor-promoting inflammation. Second, to establish how *Kras* mediates immune evasion during malignant progression, regardless of its mutation status. Skin carcinogenesis presents a unique model to study these questions, as the skin is an apt tissue to study cellular response to injury. Chemical injury, like that in the form of irritants which activate immunological responses, requires coordination between normal and immune cells which are easily captured in the skin.

In order to capture the differential roles of *Hras* and *Kras* signaling, I leveraged a dataset of over 100 chemically-induced mouse cSCCs and matched adjacent skin from a heterogenous mouse population. This dataset replicates the variability of individual tumor samples found in human cancer cohorts, due to the heterogenous genetic background of the mouse population used to induce tumors. Due to the sample size, we were able to assess covarying genes with *Hras* and *Kras* in order to understand the global differences in *Hras* and *Kras*-driven signaling. I also extended this gene co-expression approach to the analysis of samples collected over time following an exposure to a promoter. In the chapters that follow, I present the analysis of gene co-expression networks built from a) a genetically heterogeneous tumor dataset or b) perturbation over time.

With these data, we are able to document the specific roles of *Hras* and *Kras* in tumorigenesis and demonstrate that they allow keratinocytes to evade the immune system in different ways. In Chapter 2, I focus on the role of wildtype *Hras* in coordinating the inflammatory response to TPA which results in cSCCs. In Chapter 3, I focus on the role of oncogenic *Kras* in resisting host immunity to the tumor. The central theme of the work described here is in the distinct roles of *Hras* and *Kras* in controlling responses to the immune cells present in during tumor promotion and malignant progression.

Chapter 2: *Hras* mitigates innate immunity during TPA-driven tumor promotion in cSCC

Abstract

Normal tissue is constantly exposed to and responding to diverse environmental insults, some of which are mutagenic and some of which are promoting. We sought to understand the ability of a tumor promoter to select a specific mutant clone, using the well characterized tumor promoter TPA (12-O-tetradecanoylphorbol-13-acetate). It is not yet clear why TPA preferentially induces the proliferation of oncogenic *Hras* clones following DMBA (7,12-Dimethylbenzanthracene)-driven mutagenesis, given that oncogenic *Kras* clones can also be induced in a permissive setting[2]. Here we show that the normal tissue response to TPA reflects the specific functions driven by oncogenic *Hras* or *Kras*, demonstrating a clear connection between the mutant cell's fitness for a new environment. In normal skin which preferentially gives rise to oncogenic *Hras*-driven tumors, we found that TPA induced dermal-specific wound resolution processes which are activated in those tumors. In normal skin which preferentially gives rise to oncogenic *Kras*-driven tumors, we found that TPA induced cell replication programs which are activated in those tumors. Our results suggest that the environment induced by an inflammatory stimulus, like TPA, directly selects for the a priori mutant cell, promoting it towards a neoplasm. We thus demonstrate here, for the first time, a direct relationship between a tumor promoter and the selected tumor initiating clone. As we continue to identify and define naturally occurring tumor promoters, this work sets the stage for drawing the connection between tumor promoters and the tumors they drive.

Introduction

Chronic inflammation is associated with tumor incidence across many tissues. There are many types of inflammatory stimuli, and it is not yet clear how different chemical tumor promoters may drive selection of specific mutant cells. A widely used chemical tumor promoter is TPA (12-O-tetradecanoylphorbol-13-acetate), which promotes a mouse model of cutaneous squamous cell carcinoma (cSCC). TPA canonically promotes cSCCs driven by an oncogenic mutation in *Hras*, and these carcinomas first present as papillomas which later progress into cSCCs. Interestingly, while TPA can still promote cSCCs in mice with germline loss of *Hras*, it is far less efficient at promoting papillomas in these mice[2].

The combination of events leading to selection of a particular clone can result from a number of factors including the environment stimulus. In the event of specific change in the environment, the optimal features necessary to survive will change, thus causing a shift in which cells are selected to survive. The two-step chemical carcinogenesis model[15] in this study has the advantage of a genetically-diverse population of cells where we can observe natural processes of selection. Therefore, it affords an optimal opportunity to understand how a specific environmental stimulus can select for a specific mutant clone.

The sequences of *Hras* and *Kras* differ only in the C-terminal region, sharing almost 90% homology. The C-terminal hypervariable region contains post-translational modifications which may alter downstream signaling consequences. Downstream signaling is also thought to be impacted by differential subcellular localization to other membrane organelles in the cell, like the Golgi or endoplasmic reticulum (ER)[16,17]. However, the impact of the signaling differences on fitness within an inflammatory environment that promotes tumors have not been fully explored yet.

The biological functions of *Hras* are often described in the context of overexpression or oncogenic signaling compared to oncogenic mutations in *Kras*. However, given the differences noted in TPA promoted cSCC which are *Hras* or *Kras* mutant, we sought to further clarify their homeostatic roles. We reasoned that tumor promotion must be taking advantage of functions driven by each of these oncogenes in a specific manner, given that DMBA + TPA overwhelmingly selects for these mutations in specific environments. We thus set out to understand the *Hras*-dependent and *Kras*-dependent mechanisms of TPA promotion and how their functions contribute to the normal tissue response to an environmental perturbation.

Results

TPA induces inflammation and proliferation in Hras WT and KO skin

Tumors induced by DMBA + TPA on an *Hras*^{-/-} background arise with different dynamics as compared to WT FVB mice: while papilloma growth over the same period of time is far lower in the absence of *Hras*, the carcinoma incidence rate is similar[2]. This suggests that the role of *Hras* may be important for the response to TPA in normal tissue, even though the consequences of its oncogenic activation may be partially rescued by other oncogenes like *Kras*. We thus set out to characterize the cutaneous response to TPA and to assess the role of *Hras* in this process.

First, we assessed the TPA effect at an acute resolution across multiple timepoints within one week of exposure to TPA. We profiled dorsal mouse skin exposed to TPA by RNA-seq at multiple early and late time points known to reflect the immediate effect of TPA[18], in both wild-type FVB and *Hras*^{-/-} mice (**Figure 2.1.1**). From there, we identified TPA responsive genes (TRGs) at each point in time by constructing modules of genes whose expression strongly correlated to every other gene (**Figure 2.1.2)**. Rather than asking which genes are differentially expressed between each sequential timepoint, constructing gene expression modules by correlating genes across a feature (e.g. time of exposure to a chemical) allows us to specifically address functions

which change at specific points in time. We applied a regression against the kME for each module in a network to the timepoint in order to identify the timepoint responsive genes (TRGs) at each time point, and functionally analyzed the TRGs by gene set enrichment analyses. We found that the acute response to TPA is initiated by rapid epidermal differentiation and inflammation, followed by proliferation and wound resolution (**Figure 2.1.3**). We also compared our unbiased RNAseq analysis with existing literature on TPA response in mouse skin. Here, we found that the genes strongly downregulated in response to TPA were enriched for a small gene set identified to be downregulated 6 hours after TPA treatment[19]. This provided confidence that our gene expression module based identification of TRGs at each timepoint was a refined and specific method to interrogate the biology in this timecourse.

The inflammation and proliferation that is characteristic of the TPA response (**Figure 2.1.3)** is initially induced at 12 hours (**Figure 2.1.4)** and 24 hours (**Figure 2.1.5**) post TPA exposure, respectively. Since these processes are necessary for TPA to induce malignant transformation of initiated cells, we asked what the role of *Hras* is in the TPA-induced inflammation and proliferation. We treated *Hras*^{-/-} mice with one exposure to TPA and performed a similar gene-expression module analysis to identify the TRGs at each timepoint. We found that *Hras*^{-/-} animals enriched their inflammatory response at 2 hours, far earlier than the 12 hours it takes in WT FVB animals (**Figure 2.1.6**). Even in the absence of *Hras*, proliferation remained induced most strongly at 24 hours, suggesting that normal *Hras* does not have a role in coordinating cell cycle functions (**Figure 2.1.7**).

Hras is required for epidermal differentiation induced by tumor promotion in skin

The conservation in enriched proliferation functions at 24 hours led us to ask how the TRGs were conserved at each timepoint. Interestingly, we saw that less than 25% of the genes induced in WT mice at the 24 hour timepoint were also induced at this timepoint in *Hras*^{-/-} animals.

In contrast, the timepoint with the highest overlap in TRGs was 6 hours with almost 80% of genes conserved. In wildtype animals, *Hras* expression at 6 hours after TPA exposure is not different from baseline expression (**Figure 2.2.1**), which led us to ask if the functions enriched at 6 hours were *Hras* independent functions which are conserved in the TPA response. We found that Myc targets and ribosome processes were enriched in both WT and *Hras*^{-/-} animals at 6 hours after TPA exposure (**Figure 2.2.2, Figure 2.2.3**). While many of the enriched functions were conserved, we noted that keratinization processes were specifically enriched in the WT TPA response, and not in the *Hras*^{-/-} animals (**Figure 2.2.2, Figure 2.2.4**). Previously, we had also seen that the epidermal development processes related to keratinization were all enriched beginning at 6 hours of TPA exposure and continued through 72 hours following TPA exposure (**Figure 2.2.4**). To further assess the role of *Hras* in the epidermal development processes induced by TPA, we asked if the TRGs at each timepoint in WT and *Hras*^{-/-} animals were enriched for a selection of genesets reflecting this biology. We found that in animals lacking *Hras*, the keratinization and epidermal differentiation processes normally induced by TPA were largely not enriched (**Figure 2.2.4**). This led us to conclude that *Hras* may be necessary for epidermal differentiation which leads to cSCC formation.

Although there have been reports on how oncogenic *Hras* populations are tolerated and maintained in the skin epithelium[20,21], the role of WT *Hras* has not previously been described with important roles for skin homeostasis. To understand this further, we asked which genes *Hras* expression correlated with in tumor adjacent skin from mice treated with DMBA + TPA for 20 weeks. This cohort of 95 animals represent an F1 cross between FVB and Spretus mice, providing background heterogeneity which can be exploited by gene expression correlation analysis[13]. We reasoned that the genes correlated to *Hras* expression in the tumor adjacent dorsal skin would again represent the homeostatic functions of *Hras* in the skin. Here, we found that the genes significantly positively correlated with *Hras* were most significantly enriched for epidermal

development and differentiation (**Figure 2.2.5**). Interestingly, there are also multiple enrichments for epithelial cell differentiation and development, along with hair follicle development (**Figure 2.2.5**). This points to a general role of *Hras* across multiple tissues which is worth exploring further in order to understand tumor biology.

Promotion enhances Kras-driven cell proliferation responses

We then asked which programs were enriched in the *Hras*$^{-/-}$ TPA response and missing in the WT, and found that cell replication processes were more strongly enriched in *Hras*$^{-/-}$ animals than WT (**Figure 2.3.1**). As cell replication programs are associated to *Kras* activity, we assessed the *Kras* expression levels in response to TPA. Regardless of the *Hras* status, there was a surprisingly similar increase in *Kras* expression in response to TPA (**Figure 2.3.2**). While the change in *Kras* expression itself was not differentially affected between the WT and *Hras*$^{-/-}$, we explored the possibility of *Kras* signaling components being affected. Here, we found that the average expression of the Hallmark geneset positively associated to *Kras* signaling was induced in the *Hras*$^{-/-}$ mice, but not WT (**Figure 2.3.3**). This indicates that *Kras* is being both induced and activated in the *Hras*$^{-/-}$ response to TPA, though in the WT it is not activated. This further underlines the activity of *Kras* dependent processes being activated in response to TPA in the tissue which gives rise to *Kras* mutant cSCC, providing an explanation for *Kras* mutant clones being selected by TPA.

When defining the TPA response by gene expression modules, we see that beginning at 12 hours the TPA response is no longer maintained in the *Hras*$^{-/-}$ animals. The TPA response is canonically characterized by the strong induction of skin development and epidermal processes, which are not maintained in *Hras*$^{-/-}$ animals. Conversely, the cell replication and cell cycle programs canonically attributed to *Kras* signaling are induced by TPA in the *Hras*$^{-/-}$ animals, which produce oncogenic *Kras* cSCCs.

We again assessed the tumor-adjacent skin from mice bearing either *Hras* mutant or *Kras* mutant cSCC, and compared the genes co-expressed with *Kras* in either group. Here, we found a remarkable conservation in the function performed by *Kras* in tumor-adjacent skin, regardless of the background context (**Figure 2.3.4, Figure 2.3.5**). Rather than acquiring new functions or compensating for other functions, it seems *Kras* performs similar functions in tumor promotion, regardless of its oncogenic status.

Hras inhibits innate immune responses induced by TPA

Finally, we observed an enrichment in the genes anti-correlated with *Hras* in tumor-adjacent skin of WT animals (**Figure 2.4.1**) for leukocyte migration and cytokine signaling. To reconcile this finding with the enrichment of inflammatory processes induced by TPA in WT animals (**Figure 2.1.6**), we compared the enrichment of inflammatory processes in WT and *Hras*$^{-/-}$ animals induced by TPA. Here, we found a dramatic increase in the enrichment of inflammatory signals in the absence of *Hras* (**Figure 2.4.2**), beginning at 2 hours after TPA exposure and continuing through 12 hours. In order to define the inflammatory response to TPA and its dependence on *Hras*, we then performed an in silico deconvolution[22] of the leukocytes present in each sample. Here, we identified key immune cell populations which were differentially responsive in the WT or *Hras*$^{-/-}$ setting. We found that activated dendritic cells, neutrophils, and activated memory CD4 T cells were all activated in the absence of *Hras*, indicating increased efficiency in patrolling for and clearing mutant cells (**Figure 2.4.3**). Furthermore, regulatory T cells were only induced in the WT animals, suggesting a role for *Hras* in recruiting Tregs to the inflammatory environment as well (**Figure 2.4.3**). From these results we conclude that the TPA response also requires epidermal expression of *Hras* for responding to signals produced by immune cells which are recruited to the site of TPA-induced injury.

Figures
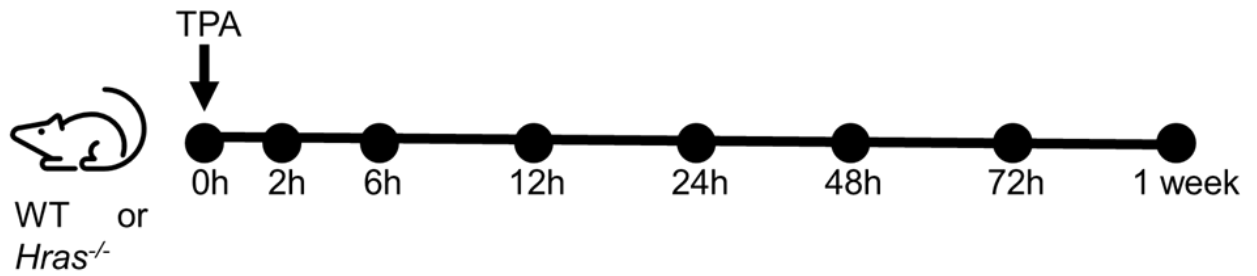
Figure 2.1.1 Experimental design for promoter timecourse.

In 5 male and 5 female WT and *Hras*$^{-/-}$ mice, we treated the dorsal skin of shaved mice with a single dose of TPA. Dorsal skin was collected at each indicated point in time following TPA exposure.
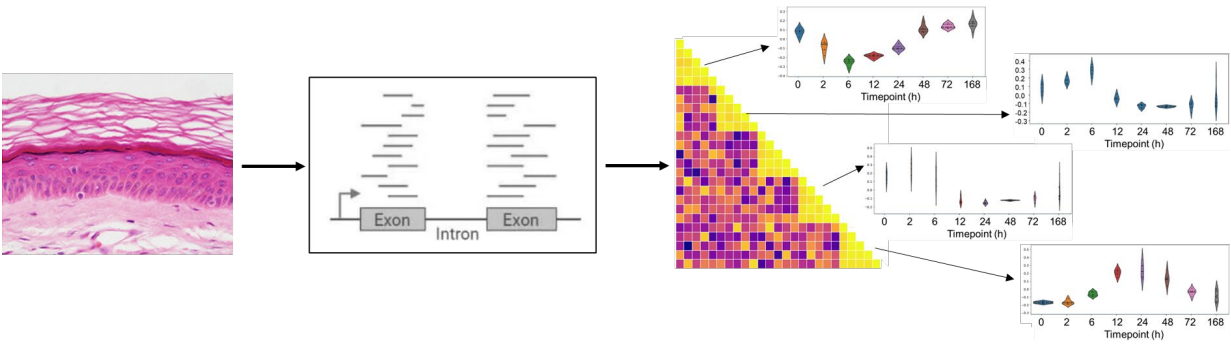
Figure 2.1.2 Sample processing and analytical workflow

Dorsal skin was collected and processed for RNA isolation and measured by RNAseq. Genes were grouped into co-expression modules by calculating the correlation in expression across all samples within a timecourse. Representative examples of TPA responsive modules at each time point are depicted. These were determined by plotting the module eigengene for each sample and identifying modules which were highly expressed at only one timepoint. The genes which constitute each module are then functionally assessed by gene set enrichment analyses.
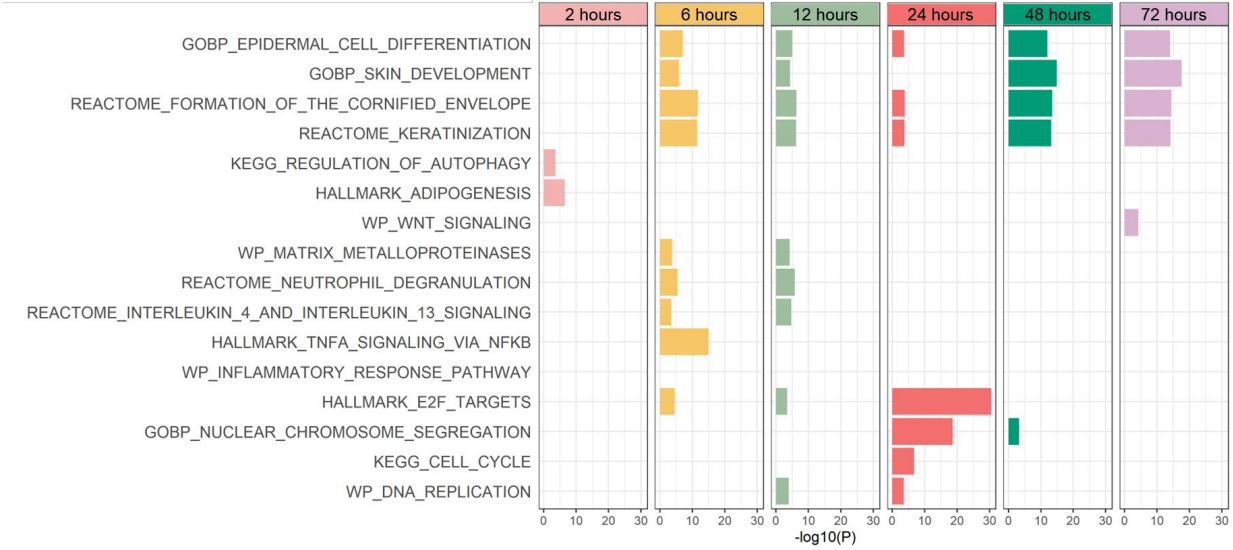
Figure 2.1.3 GSEA over time, TPA timecourse in FVB animals

Geneset enrichment significances are depicted for the TPA responsive genes (TRGs) at each timepoint in FVB animals. These represent the strongest enriched functions identified at each timepoint, and their enrichments across the timecourse.

GSEA at 12 hours in WT animals

Figure 2.1.4 Inflammatory functions enriched at 12 hours after TPA response in WT animals Strongest geneset enrichments for TPA responsive genes at 12 hours in FVB/WT animals, with inflammatory functions marked.

GSEA at 24 hours in WT animals
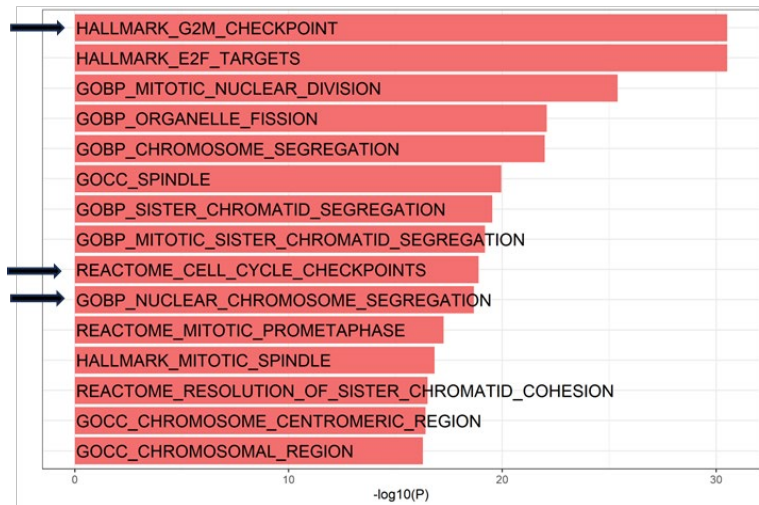
Figure 2.1.5 Proliferation functions enriched at 24 hours after TPA response in WT animals
Strongest geneset enrichments for TPA responsive genes at 24 hours in FVB/WT animals, with
proliferation functions marked.

GSEA at 2 hours in Hras KO animals

REACTOME_SIGNALING_BY_INTERLEUKINS
HALLMARK_APOPTOSIS
GOBP_RESPONSE_TO_TUMOR_NECROSIS_FACTOR
WP_TOLLLIKE_RECEPTOR_SIGNALING_PATHWAY
KEGG_TOLL_LIKE_RECEPTOR_SIGNALING_PATHWAY
GOMF_CYTOKINE_RECEPTOR_BINDING
WP_TNF_ALPHA_SIGNALING_PATHWAY
GOBP_ERK1_AND_ERK2_CASCADE
HALLMARK_IL6_JAK_STAT3_SIGNALING
REACTOME_INTERLEUKIN_10_SIGNALING
GOMF_DNA_BINDING_TRANSCRIPTION_ACTIVATOR_ACTIVITY
GOBP_RAS_PROTEIN_SIGNAL_TRANSDUCTION
GOBP_REGULATION_OF_EPITHELIAL_CELL_MIGRATION
KEGG_CYTOKINE_CYTOKINE_RECEPTOR_INTERACTION
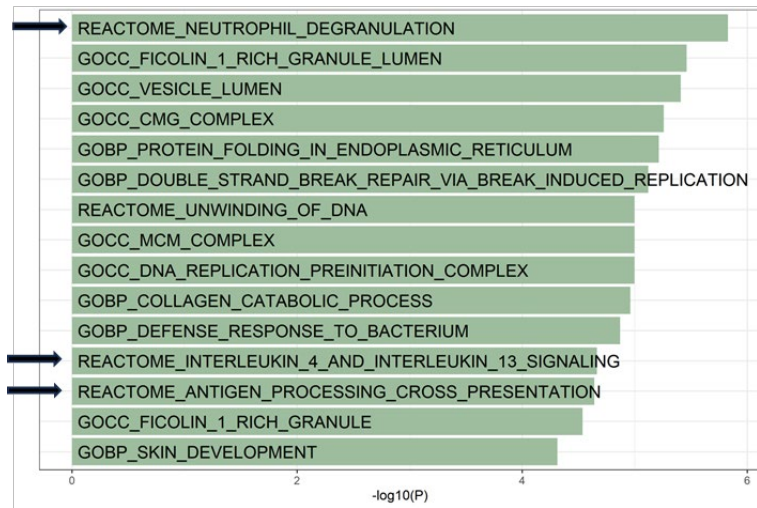WP_IL18_SIGNALING_PATHWAY

-log10(P)

Figure 2.1.6 Inflammatory functions enriched at 2 hours after TPA response in *Hras*-/- animals Strongest geneset enrichments for TPA responsive genes at 2 hours in *Hras*-/- animals, with inflammatory functions marked.
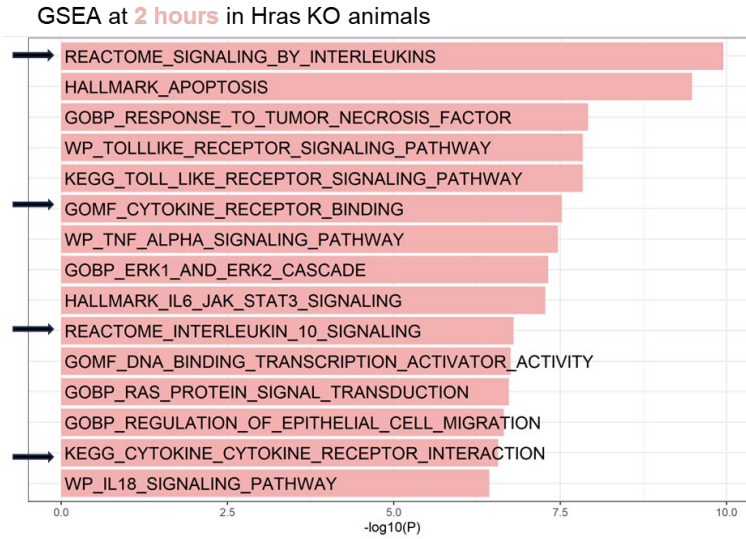
GSEA at 24 hours in Hras KO animals

REACTOME_MITOTIC_PROMETAPHASE
HALLMARK_E2F_TARGETS
GOCC_CONDENSED_CHROMOSOME_CENTROMERIC_REGION
REACTOME_RHO_GTPASES_ACTIVATE_FORMINS
REACTOME_SEPARATION_OF_SISTER_CHROMATIDS
GOBP_MICROTUBULE_CYTOSKELETON_ORGANIZATION_INVOLVED_IN_MITOSIS
REACTOME_RHO_GTPASE_EFFECTORS
REACTOME_CELL_CYCLE_CHECKPOINTS
GOBP_CENTROMERE_COMPLEX_ASSEMBLY
GOBP_MITOTIC_SPINDLE_ORGANIZATION
HALLMARK_MITOTIC_SPINDLE
GOBP_REGULATION_OF_CHROMOSOME_SEPARATION
REACTOME_SIGNALING_BY_RHO_GTPASES
GOBP_REGULATION_OF_MITOTIC_NUCLEAR_DIVISION
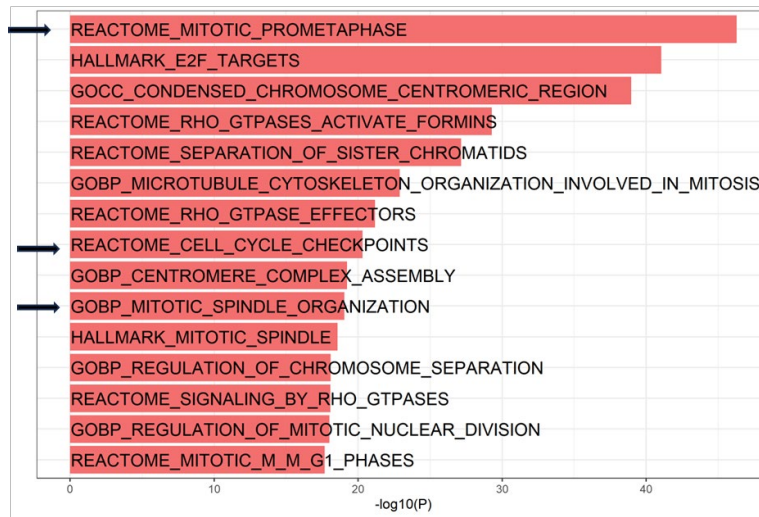REACTOME_MITOTIC_M_M_G1_PHASES

-log10(P)

Figure 2.1.7 Proliferation functions enriched at 24 hours after TPA response in *Hras*$^{-/-}$ animals Strongest geneset enrichments for TPA responsive genes at 24 hours in *Hras*$^{-/-}$ animals, with proliferation functions marked.
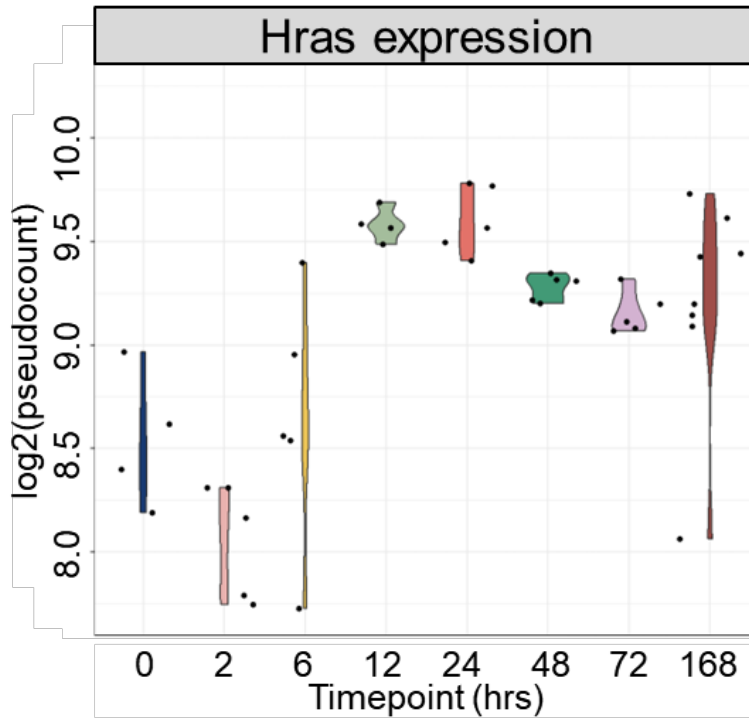
Figure 2.2.1 *Hras* expression in response to TPA in WT animals

GSEA at 6 hours in Hras WT animals

HALLMARK_MYC_TARGETS_V2
REACTOME_FORMATION_OF_THE_CORNIFIED_ENVELOPE
REACTOME_KERATINIZATION
GOBP_KERATINIZATION
HALLMARK_MYC_TARGETS_V1
GOBP_RIBOSOME_ASSEMBLY
GOBP_HEMATOPOIETIC_STEM_CELL_DIFFERENTIATION
WP_PHOTODYNAMIC_THERAPYINDUCED_UNFOLDED_PROTEIN_RESPONSE
GOBP_CELLULAR_RESPONSE_TO_TOPOLOGICALLY_INCORRECT_PROTEIN
GOCC_ENDOPLASMIC_RETICULUM_CHAPERONE_COMPLEX
GOBP_EPIDERMIS_DEVELOPMENT
GOBP_HEMATOPOIETIC_PROGENITOR_CELL_DIFFERENTIATION
HALLMARK_TNFA_SIGNALING_VIA_NFKB
GOBP_REGULATION_OF_HEMATOPOIETIC_STEM_CELL_DIFFERENTIATION
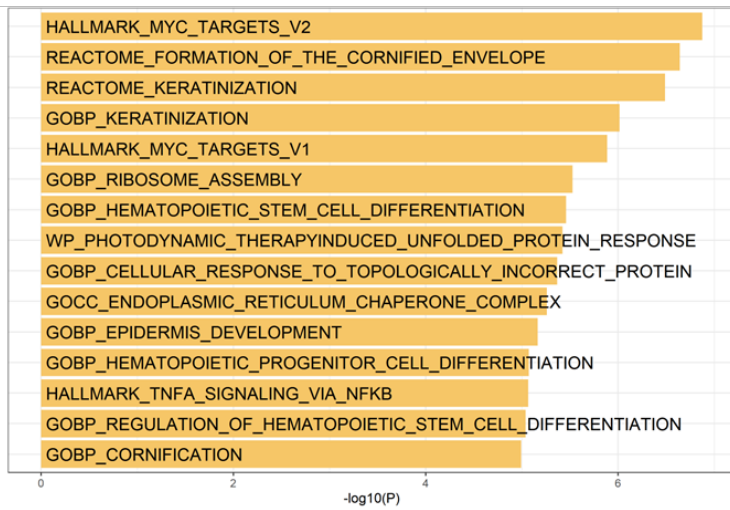GOBP_CORNIFICATION

-log10(P)

Figure 2.2.2 GSEA at 6 hours post TPA exposure in *Hras* WT animals

Strongest geneset enrichments for TPA responsive genes at 6 hours after exposure in WT animals.
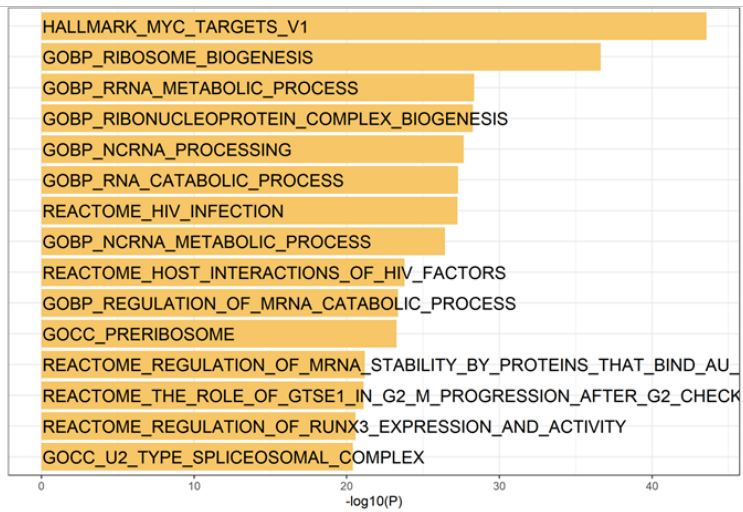
GSEA at 6 hours in Hras KO animals

HALLMARK_MYC_TARGETS_V1	
GOBP_RIBOSOME_BIOGENESIS	
GOBP_RRNA_METABOLIC_PROCESS	
GOBP_RIBONUCLEOPROTEIN_COMPLEX_BIOGENESIS	
GOBP_NCRNA_PROCESSING	
GOBP_RNA_CATABOLIC_PROCESS	
REACTOME_HIV_INFECTION	
GOBP_NCRNA_METABOLIC_PROCESS	
REACTOME_HOST_INTERACTIONS_OF_HIV_FACTORS	
GOBP_REGULATION_OF_MRNA_CATABOLIC_PROCESS	
GOCC_PRERIBOSOME	
REACTOME_REGULATION_OF_MRNA_STABILITY_BY_PROTEINS_THAT_BIND_AU_	
REACTOME_THE_ROLE_OF_GTSE1_IN_G2_M_PROGRESSION_AFTER_G2_CHECK	
REACTOME_REGULATION_OF_RUNX3_EXPRESSION_AND_ACTIVITY	
GOCC_U2_TYPE_SPLICEOSOMAL_COMPLEX	

-log10(P)

Figure 2.2.3 GSEA at 6 hours post TPA exposure in *Hras*-/- animals

Strongest geneset enrichments for TPA responsive genes at 6 hours after exposure in *Hras*-/- animals
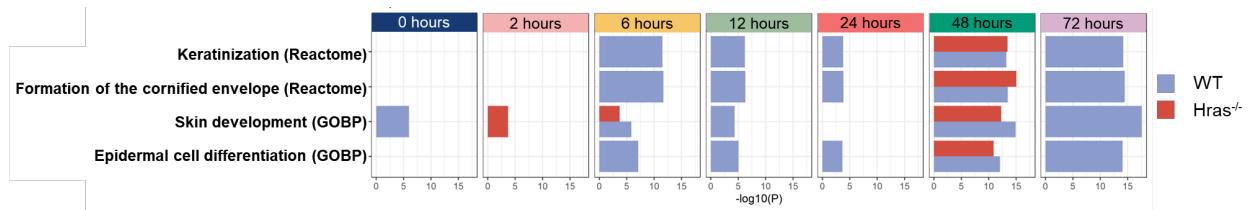
Figure 2.2.4 Epidermal differentiation related processes induced by TPA in WT and *Hras*^{-/-} animals

Comparison of epidermal development geneset enrichment significances of TPA responsive genes at each indicated timepoint, between WT and *Hras*^{-/-} animals.
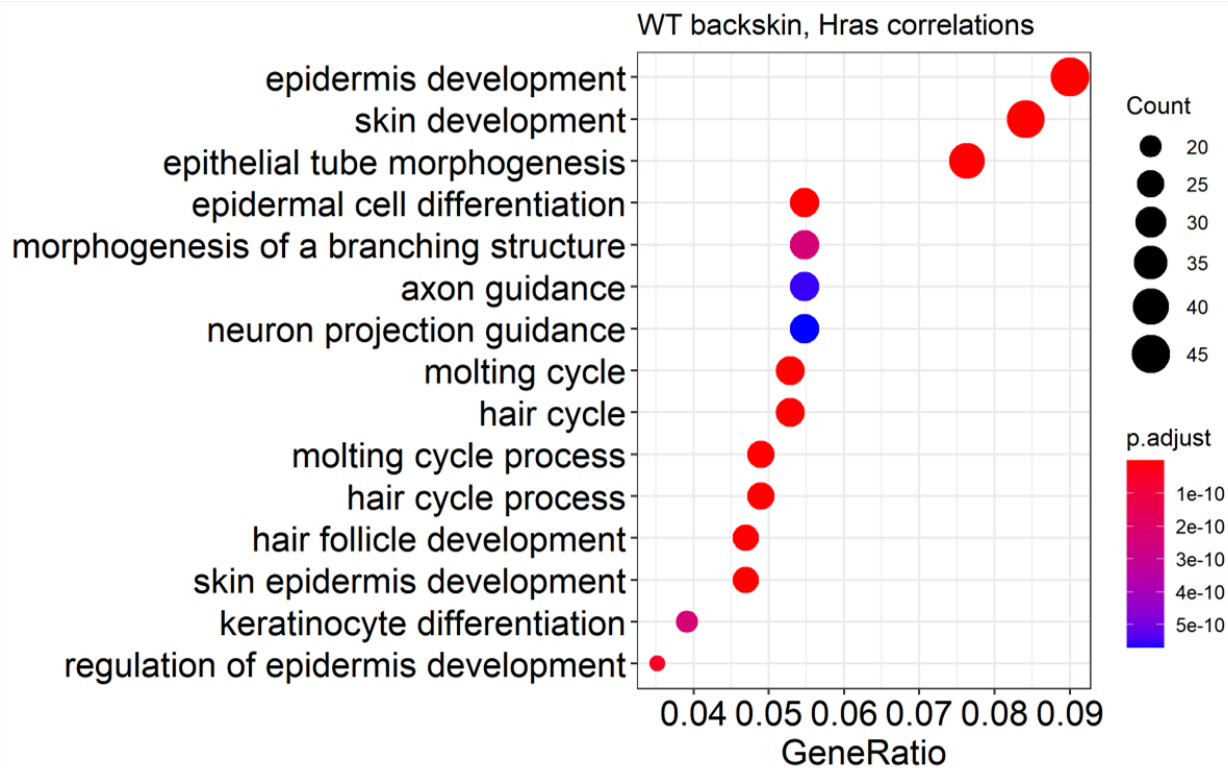
Figure 2.2.5 Positive *Hras* correlations in tumor adjacent skin from WT animals
Bulk gene expression analysis of 95 tumor adjacent skin samples from 95 WT mice treated with DMBA and 20 weeks of TPA. Gene ontology enrichments depicted for the 595 genes positively correlated with *Hras* (q<0.001, ρ > 0.5).
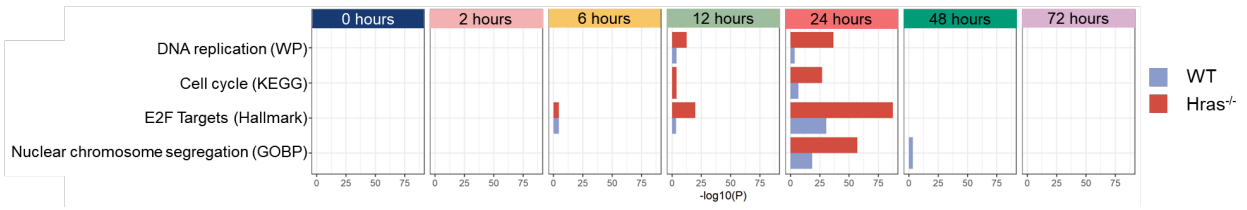
Figure 2.3.1 Cell proliferation processes induced by TPA in WT and *Hras*-/- animals
Comparison of cell proliferation geneset enrichment significances of TPA responsive genes at each indicated timepoint, between WT and *Hras*-/- animals.
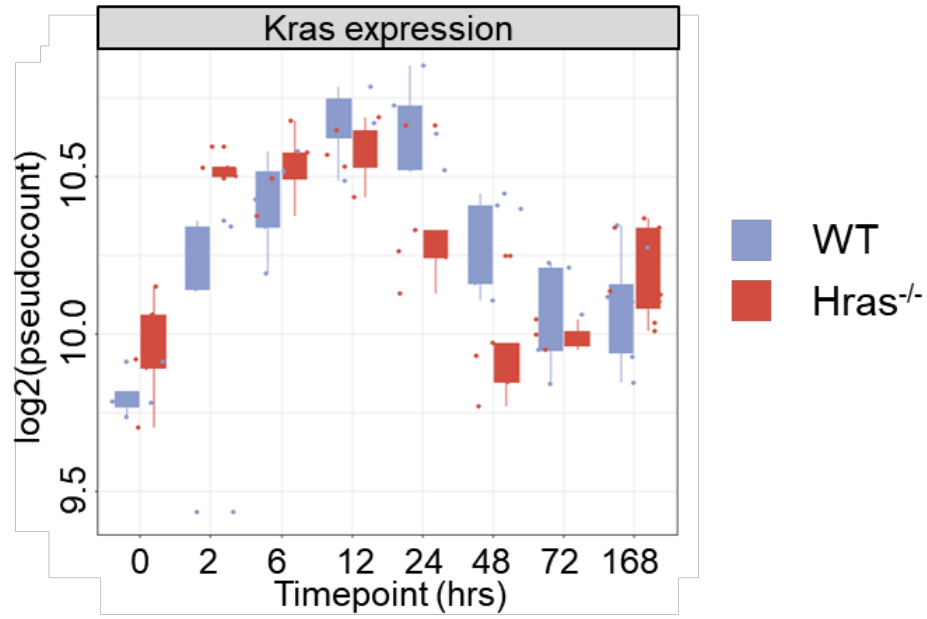
Figure 2.3.2 *Kras* expression after TPA exposure in WT and *Hras*^{-/-} animals
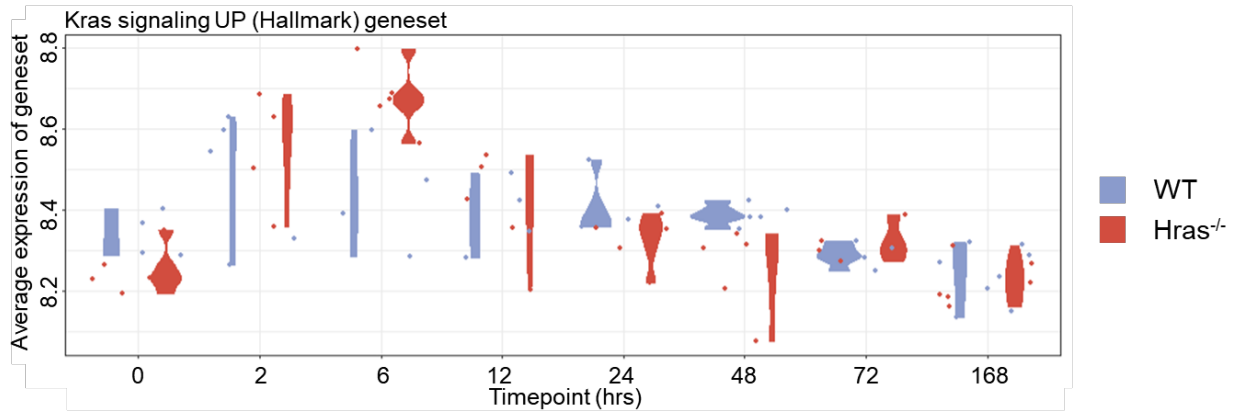
Figure 2.3.3 Average expression of Hallmark *Kras* signaling geneset in WT and *Hras*^{-/-} animals.

Within each sample, the average expression of all the genes represented by the *Kras* Signaling UP Hallmark genset is represented here. WT shown in purple, *Hras*^{-/-} shown in red.

Figure 2.3.4 Positive *Kras* correlations in tumor adjacent skin from WT animals
Bulk gene expression analysis of 95 tumor adjacent skin samples from 95 WT mice treated with DMBA and 20 weeks of TPA. Gene ontology enrichments depicted for the 768 genes positively correlated with *Kras* (q < 0.001, ρ > 0.5).
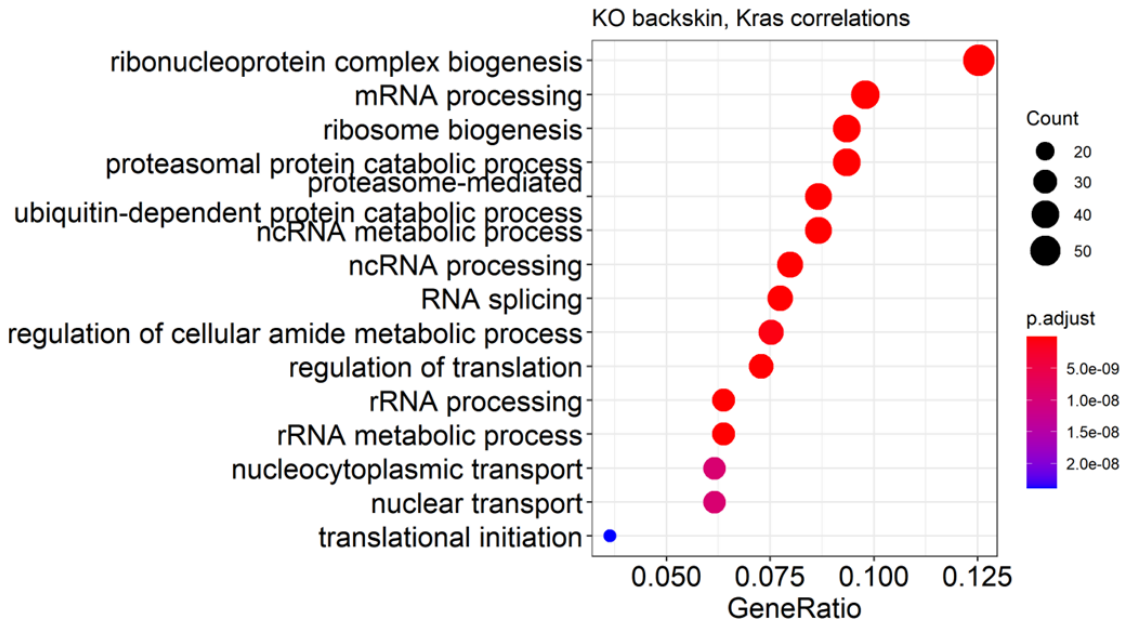
Figure 2.3.5 Positive *Kras* correlations in in tumor adjacent skin from *Hras*^{-/-} animals
Bulk gene expression analysis of 90 tumor adjacent skin samples from 90 *Hras*^{-/-} mice treated with DMBA and 20 weeks of TPA. Gene ontology enrichments depicted for the 458 genes positively correlated with *Kras* (q < 0.001, ρ > 0.5).
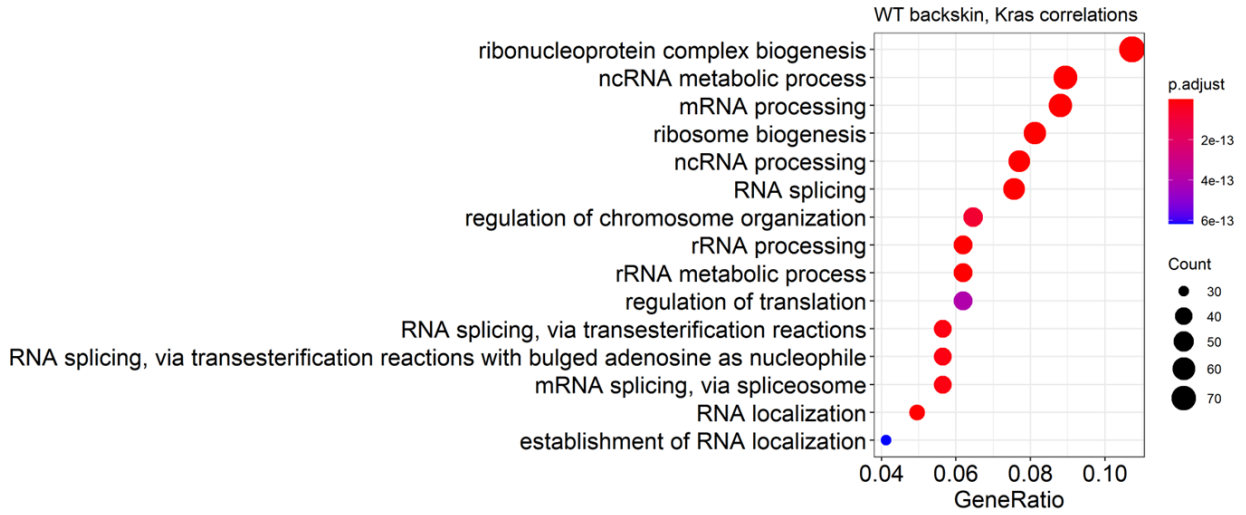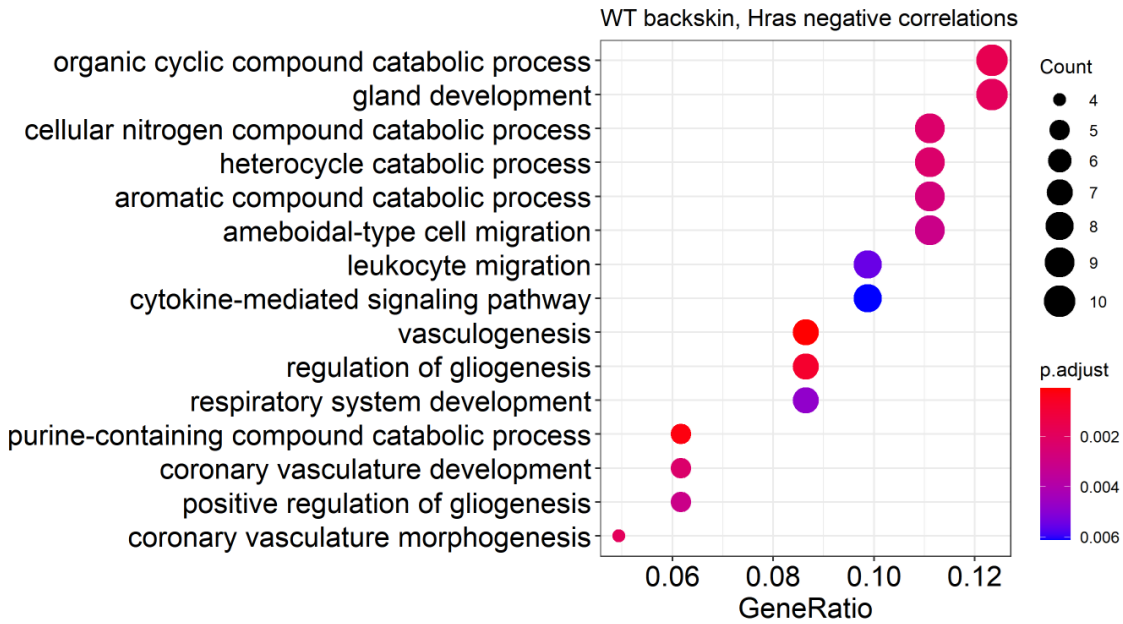
Figure 2.4.1 Negative *Hras* correlations in tumor adjacent skin from WT animals
Bulk gene expression analysis of 95 tumor adjacent skin samples from 95 WT mice treated with
DMBA and 20 weeks of TPA. Gene ontology enrichments depicted for the 90 genes negatively
correlated with *Hras* (q <0.001, ρ < -0.5).
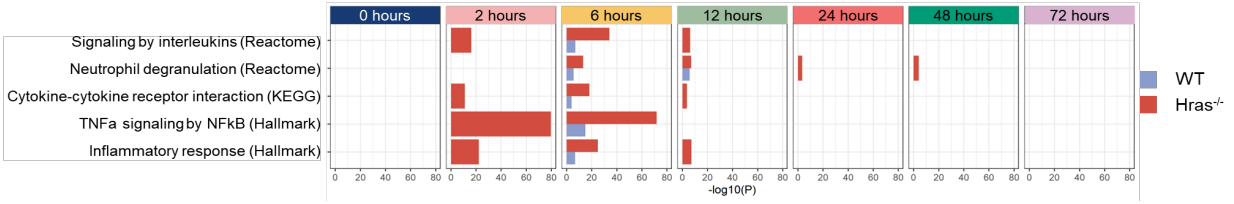
Figure 2.4.2 Inflammatory processes induced by TPA in WT and *Hras*-/- animals
Comparison of inflammatory geneset enrichment significances of TPA responsive genes at each
indicated timepoint, between WT and *Hras*-/- animals.

Figure 2.4.3 Immune cell types induced by TPA in WT or *Hras*^{-/-} animals

In silico deconvolution of immune cell presence by CIBERSORT identified cell types whose induction in response to TPA is dependent on *Hras*

Discussion

In this study, we report the distinct roles of *Hras* and *Kras* in tumor promotion by TPA. We show that the roles played by each oncogene in normal tissue align with the functions mediated by the transformed oncogene in their respective tumor and provide a clear connection 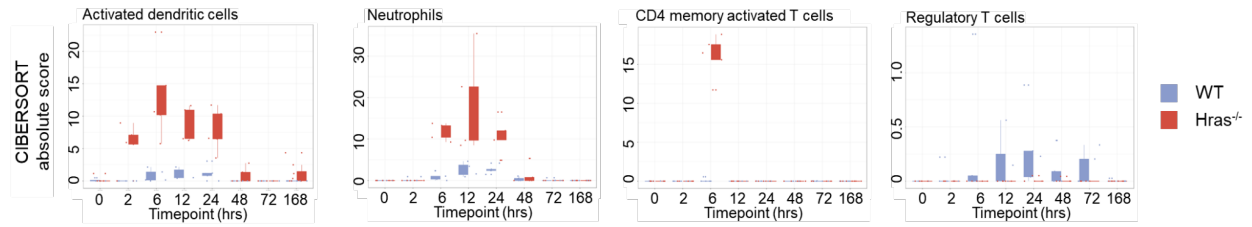between an environmental stimulus and the selection of a mutant clone. We also define the *Hras*-dependent mechanisms of the canonical TPA response which leads to papillomas, demonstrating why fewer papillomas are induced in the absence of *Hras*.

We show that *Hras* drives epidermal differentiation and keratinization processes in both normal and oncogenic settings, which is induced by TPA. As the oncogenic activation of *Hras* leads to constitutive activation of *Hras* signaling, we show here that TPA induces keratinization processes which are necessary for malignant transformation to papillomas. This may provide the basis for understanding tissue specific oncogenic activity of *Hras*, as it may not be advantageous for other tissues or cell types to transform with increased epidermal differentiation functions.

We show that *Hras* diminishes the signals necessary to recruit immune cells responsible for patrolling and clearing mutant clones. Not only do we find the induction of dendritic cells and neutrophils in the *Hras*^{-/-} background, but we also find that *Hras*^{-/-} mice are unable to induce regulatory T cells. This difference in immune cell recruitment dependent on *Hras* signaling provides an important line of questioning for mechanisms of tumor promotion. While TPA induces keratinocyte production of inflammatory signals, the lack of *Hras* results in impaired ability to receive signals produced by the recruited immune cells. Future experiments will provide more specific understanding of the signaling axes that govern this response. In this study, we address the normal functions of *Hras*, though in the context of tumor promotion it would also be important to consider the mutant, and constitutively activated functions, of *Hras*. Prior reports of the

tolerance of oncogenic mutant clones in the skin suggests that there is an important immune evading property associated with the activation of *Hras* signaling[21].

The direct connections between *Hras* and inflammation were surprising to find so clearly in our study, and it will be necessary to continue studying the connection between *Hras* signaling and the recruitment of dendritic cells, neutrophils, and regulatory T cells. Another immune cell population we were interested in addressing in this study was macrophages. The role of macrophages in tumor promotion has been explored for many decades, though recently as a source of tumor promoting IL-1B [23]. In *Hras*^{-/-} tumor adjacent skin, we find far fewer macrophages, which aligns with its reduced propensity for TPA-induced tumorigenesis. Furthermore, keratinization signaling, including the production of keratin 8, has been reported to regulate the production of macrophage recruitment chemokines[24]. Together, this lends credence to the important role of *Hras* in mediating the tumor promoting inflammation induced by TPA in the skin.

We demonstrate that while *Kras* expression is induced by the TPA response in both the presence and absence of *Hras*, *Kras* activity and signaling is only induced in the absence of *Hras*. This suggests that *Kras* is not an essential component of the canonical TPA promotion response and perhaps provides essential processes during a later stage of tumorigenesis. In Chapter 3, I will present one possible explanation for the role *Kras* plays in engaging the immune response to tumor evolution.

Methods

Mouse handling

All mouse experiments were performed in accordance with the Institutional Animal Care and Use Committee of the University of California, San Francisco. For the TPA exposure experiments, WT FVB or *Hras*^{-/-} mice were shaved one day prior to use. Animals were 7-9 weeks of age and

randomized between the timepoint groups to avoid confounding by age. TPA was reconstituted in acetone and treated with 200µl per treatment of a 10-4M solution. The treatment was performed in light sensitive conditions until the acetone dried completely. At the designated timepoint following TPA exposure, mice were sacrificed by cervical dislocation and the dorsal skin was flash frozen in chunks for downstream processing. The central piece was fixed in 10% formalin for 24 hours on a piece of cardstock paper, then preserved in 80% ethanol until paraffin processing.

RNA isolation

Flash frozen chunks were ground into Trizol using a homogenizer and RNA was isolated by standard phenol-chloroform procedures. A standard amount of purified RNA was provided to the UCLA Technology Center for Genomics and Bioinformatics for RNAseq library preparation and sequencing. Libraries were prepared with the KAPA mRNA HyperPrep Kit and sequenced on an Illumina Novaseq X Plus.

Data processing

We performed initial quality control on the raw fastq files with fastqc in order to assess the sequencing quality and pre-processing needs. Fastq files were aligned to Mus musculus Mm39 reference genome using hisat2. The resultant sam files were converted to sorted and indexed bam files with samtools view, then samtools sort and samtools index -b. The genewise counts were then assigned with Rsubread:featureCounts.

Gene expression analysis

The featureCounts output was processed in R (4.0.5) and normalized by DESeq2. To assign timepoint responsive genes, we utilized the FindModules function as previously described [25]. Briefly, genome-wide gene coexpression analysis was performed by calculating biweight midcorrelations using WGCNA:bicor. Genes were then hierarchically clustered with flashClust,

using 1-bicor to measure distance. The resulting dendrogram was cut at a height corresponding to the top 2% of all bicor values. Clusters containing at least 10 genes were identified and assigned a module eigengene. If the Pearson correlation of any two modules was greater than 0.85, those modules were combined iteratively until no pairs of modules met this similarity parameter. To identify timepoint responsive modules, the module eigengene was regressed with a quadratic model against the timepoints and the significant modules were reported for each timepoint. The genes contained in each of these modules were collapsed into a list of genes per timepoint which were classified as "timepoint responsive genes" or TRGs. Gene set enrichment analysis was performed by testing the overlap in TRGs with published genesets, reporting the Bonferroni corrected p-value of a hypergeometric overlap test result.

Chapter 3: *In vivo* CRISPRi screen reveals *Kras*-driven resistance to anti-PD1 therapy

Abstract

Gene expression networks are richly informative sources of biological information. Quantifying variability across a large population often reveals novel insights which are not found when comparing multiple replicates between groups. To identify novel *Kras*-driven mechanisms of resistance to a-PD1 therapy, we conducted a targeted *in vivo* CRISPRi screen for sensitizers of a-PD1 in the genes closely correlated with *Kras* expression. Here, we report the design of a custom sgRNA library informed by the gene expression network of *Kras* in 67 *Kras* mutant mouse cutaneous squamous cell carcinomas. We identify novel biological functions mediated by *Kras*, which also sensitize *Kras* mutant tumors to a-PD1. Finally, we demonstrate the sensitization of *Kras* mutant tumors to a-PD1 with combinatorial targeting of *Rc3h2* or *Sgol2*. These findings will provide a rich database of functions mediated by *Kras* as well as provide direction for combinatorial therapy strategies to improve efficacy of a-PD1 against *Kras* mutant cancers.

Introduction

Immune checkpoint inhibitor (ICI) blockade therapy has been successful in a specific set of patients, leading to an increased focus on establishing predictive markers of efficacy. Of equal importance is the cohorts of patients whose tumors are largely refractory to ICI. Solid tumors with activating mutations in *Kras* are among the most difficult to treat, with low survival rates. Recent years have brought major advancements in molecularly targeting *Kras* mutant cancers, however these approaches are limited by the specific mutation which is present. Intratumoral heterogeneity often leads to resistance to molecularly targeted therapies. Additionally, *Kras* mutant tumors are widely described to be immunologically "cold", indicating a strong immunosuppressive

environment that abrogates the effect of ICI therapies, like anti-PD1 (a-PD1) therapy. Here, we sought to understand the mechanisms surrounding the immunosuppressive environment of *Kras*-mutant tumors, in order to provide avenues for sensitizing these a-PD1-resistant cancers to a widely available treatment regimen.

The Ras signaling pathway is among the most extensively studied pathways in biology and has been linked to almost every major cell biological process. *Kras* is a GTP-ase activated by growth factor signaling, responsible for activating fundamental cellular processes like cell replication, metabolism, and differentiation. These processes are not considered to be directly related to the coordination of an immunosuppressive environment, but it is possible that genes activated downstream of *Kras* may also be related to this phenotype. To identify novel *Kras*-driven immunosuppressive mechanisms, we leveraged the use of a heterogeneous backcrossed mouse population which replicates the genetic heterogeneity seen in human populations. By inducing cSCC with the standard DMBA initiation and TPA promotion in these mice, we collected a dataset of 67 biologically distinct *Kras* mutant cSCC which were profiled by bulk gene expression. This provided the basis for a novel set of genes associated to *Kras* which could be tested for their functions in conferring resistance to ICI.

A commonly used tool to systematically interrogate the effect of gene knockdown on a perturbation is a CRISPRi (CRISPR inactivation) screen, where a catalytically dead Cas9 (dCas9) nuclease is fused to a transcriptional repressor domain (KRAB)[26,27]. This fusion protein is then targeted to desired sites in the genome by sgRNAs (single guide RNAs) in a pooled library of desired sgRNAs. While large-scale screens are feasible to conduct *in vitro*, we sought to assess their feasibility *in vivo*.

This endeavor presented a few important challenges to address before conducting a systematic interrogation of *Kras*-associated genes which may drive resistance to a-PD1 therapy. First, this study required the use of a syngeneic cell line with an immunocompetent mouse model. For immunotherapeutic screens, it is necessary to perform these experiments in a syngeneic system with an intact immune system. While mouse models for commonly studied cancers are often genetically induced, with Cre-driven alterations in every cell of a given tissue, the syngeneic tumor cell lines derived from such models are not closely related to human tumors. To combat this, we employed a cell line derived from a chemical carcinogenesis model of cSCC which closely resembles the natural life history of tumorigenesis. Second, we ensured that the size of our library corresponded with the upper limit of cells we were able to inject subcutaneously, such that we achieved over 80% library retention in untreated tumors during the course of the experiment. This was required to ensure that we did not experience loss in the non-targeting guides in any of our samples. Ensuring the retention of non-targeting guides provided confidence in the true dropout rate of guides in our library, indicating sensitivity to treatment given the knockdown of a gene. Finally, we conducted our *in vivo* experiments in a mouse model which stably expresses dCas9-KRAB in the germline, allowing for immunological tolerance of the tumor cell line used in the study. Addressing these major challenges lent confidence to the *in vivo* experiment conducted with the full library of 2000 guides.

Multiple groups have now reported the feasibility of both genome wide and targeted CRISPRi screens in *in vivo* syngeneic experiments[28–31]. Due to the lack of ideal models, findings from these studies may not be recapitulated in human clinical trials, which led us to assess immunotherapy sensitizers in a well-characterized chemically-induced cutaneous squamous cell carcinoma (cSCC) model which is resistant to a-PD1 therapy[32]. In this study, we leverage a cell line derived from a chemically-induced *Kras*[MUT] cSCC, called 168 cells, which more closely recapitulates human tumorigenesis and allows us to study tumor-immune interactions in a

syngeneic model. Using this model, we describe here the implementation of a targeted CRISPRi screen conducted *in vivo*, to identify *Kras*-driven mediators of resistance to a-PD1 therapy.

Results

Gene expression network reveals Kras-driven biological functions in mouse skin SCCs

Using the two-step carcinogenesis model in mice, we generated *Kras* mutant cutaneous squamous cell carcinomas. We first apply DMBA, a mutagen, and then chronic exposure to TPA, a tumor promoter, which results in papillomas and carcinomas after 20 weeks of treatment. We generated a genetically heterogeneous mouse population which models the genetic diversity in the human population and profiled the bulk gene expression of 67 *Kras* mutant carcinomas (**Figure 3.1**). Since these tumors are derived from a genetically heterogenous population, the variation allows us to specifically narrow on biologically significant gene expression dynamics. To identify *Kras*-driven functions, we first identified the genes whose expression most strongly correlated with *Kras* expression across all 67 tumors. We found that these genes were significantly enriched for cell replication, chromosome segregation, and RNA metabolism processes (**Figure 3.1**). While we expect to see cell cycle related processes here, this set of genes strongly correlated with *Kras* suggests that there are more functions than originally thought to be associated with *Kras*.

We also wanted to corroborate the relevance of our mouse model of *Kras*-mutant cancers with *Kras*-driven human tumors. For this, we searched the literature for studies on *Kras*-mutant human cancers and found a consensus set of genes which are synthetically lethal with *Kras*. When comparing the list of genes highly correlated with *Kras* in our dataset to the genes identified as synthetic lethal with *Kras*, we found a high level of overlap and thus concluded that our model does recapitulate features of *Kras*-mutant tumors in humans (**Figure 3.2**).

While neoplastic cells carry oncogenic *Kras*, we next sought to understand the differences in *Kras* associated functions in the wild-type compared to oncogenic context. To address this, we identified the genes most strongly correlated to *Kras* expression in the adjacent normal skin to the collected cSCC. Here, we found that the functions of the genes correlated to *Kras* are conserved regardless of its oncogenic status (**Figure 2.3.5**). We concluded that the genetically diverse population of chemically-induced *Kras* mutant tumors provided specific insight into the functions driven by *Kras*.

Thus, we next asked if these genes contained previously unknown immunosuppressive functions. To do so, we conducted an *in vivo* CRISPRi screen for genes which would sensitize *Kras* mutant tumors to a-PD1 therapy. For this screen, we had a few considerations. First, we needed to optimize the number of genes in the library with the number of cells used to inoculate the subcutaneous xenograft. Second, we needed to optimize the number of guides per construct. Third, we needed a cell line model known to be resistant to a-PD1 therapy. We achieved the first two considerations by employing a dual-guide construct approach which reduced the library size in half[27]. The cell line chosen, 168 cells, are a stable cell line derived from a *Kras* mutant cSCC induced by DMBA and TPA treatment. In *in vivo* experiments, these tumor xenografts do not respond to a-PD1 therapy and thus represents a robust model system to study resistance mechanisms for this treatment (**Figure 3.3).**

aPD1 screen

A syngeneic *in vivo* CRISPRi screen has limitations including the guide library size that is possible to screen. We intended to screen 1000 genes strongly associated with *Kras* expression across the set of *Kras*[MUT] cSCC in our dataset. Upon ensuring that a divided sublibrary of 250 genes did not experience significant library drop out, we combined the sub-libraries into the final pool which we screened. These genes represent functions known to be associated with oncogenic

Kras, such as cell cycle and proliferation programs (**Figure 3.1**). It was not clear from these functions which genes may confer resistance to a-PD1, so we proceeded to perform an *in vivo* CRISPRi screen for a-PD1 sensitivity using a syngeneic system of *Kras* mutant cSCC cells expressing dCas9KRAB, and mice with germline expression of dCas9KRAB (**Figure 3.4)**. We saw that the negative control genes were centered on a neutral effect and used the lower limit of their effects to define the hits with a sensitizing effect in this screen (**Figure 3.5**). The genes which had a significant sensitizing effect and are not considered essential genes for cell growth were then chosen as our hits.

We found that these genes were significantly enriched for functions in mRNA processing, gene expression regulation, mitochondrial processes, and chromatin. This was striking as this represents a dramatic shift in enrichment from the functions represented in the entire library. To further assess the potential roles of *Kras*, we looked at the overlap in the genes contained in the *Kras* module in *Kras*^MUT carcinomas and *Hras*^MUT carcinomas. We asked which functions are merely enhanced in the oncogenic setting but are still present in the wildtype context, and this also resulted in mRNA processing, gene expression regulation, mitochondrial processes, and DNA metabolism (**Figure 3.6**). We took this to indicate that these functions can be uniquely tied to immunosuppressive functions driven by *Kras*.

We were intrigued by the result of gene expression regulation and metabolic processes being sensitizing to a-PD1 therapy, and chose to validate four significant hits from this screen (**Figure 3.7)**. First, we generated individual knockdown cell lines using the dual guide constructs from the guide library used in the screen. This resulted in two independent cell lines per gene knockdown. These results were compared with a cell line expressing one of the non-targeting guides as the control. After confirming that the *Kras* mutant cSCC cell line expressing dCas9KRAB (168-d9K) could be used to generate individual gene knockdown cell lines, we

proceeded to *in vivo* validation of the a-PD1 sensitization of these knockdowns. Here, we found that the most significant replicated hits were Roquin2 (*Rc3h2*) and Shugoshin2 (*Sgol2*).

Validation of Sgol2 and Rc3h2 as sensitizers of a-PD1 therapy

Shugoshin2, or Sgol2, is a centromeric protein involved in chromosomal segregation. Its roles in tumor biology have been demonstrated in tumor proliferation[33] and even increased expression in tumors displaying immune evasion[34]. We demonstrate that *Kras* mutant cSCC cells with *Sgol2* knockdown are specifically sensitive to a-PD1 treatment (**Figure 3.8**) by showing the reduction in tumor volumes in knockdown cells following treatment, which is not seen in the parental cell line (**Figure 3.3**). We also demonstrate a complete response within two weeks following the final treatment dose, in 5 animals treated with a-PD1 (**Figure 3.9**). This strong validation of the results from the pooled CRISPRi screen is encouraging and will set the stage for future mechanistic validation experiments as well.

Roquin2 has functions described in differentiation helper T cells to follicular helper T cells[35], and is described as an E3 ubiquitin ligase as well as an mRNA repressor via long noncoding RNA functions[36,37]. Given that the functions have not been described in epithelial cells, we were intrigued by this hit. We demonstrate the validation of this hit from the CRISPRi screen as well, through a complete response within two weeks following the final treatment dose, in seven of the a-PD1 treated animals carrying 168-dCas9KRAB-sgRc3h2 cells (**Figure 3.10**). These experiments demonstrate the robust validation of the phenotype measured in the pooled, targeted CRISPRi screen for sensitizers of a-PD1 which are driven by *Kras*.
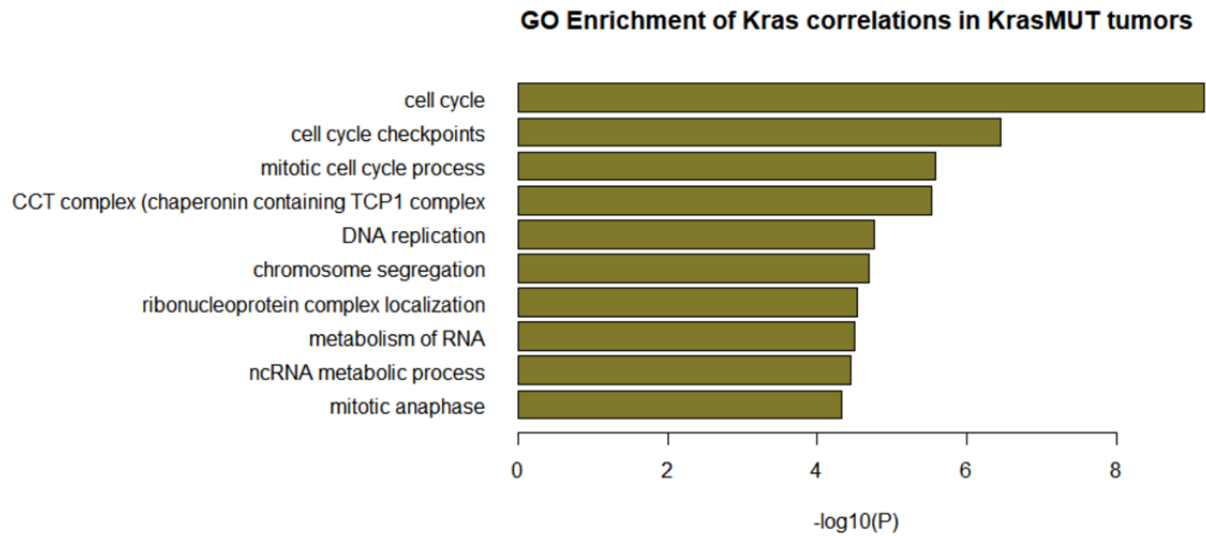
GO Enrichment of Kras correlations in KrasMUT tumors

Figure 3.1 Positive *Kras* correlations in *Kras* mutant tumors

Bulk gene expression analysis of 67 cSCC samples from 67 *Hras*^{-/-} mice treated with DMBA and 20 weeks of TPA. Gene ontology enrichments depicted for the 975 genes positively correlated with *Kras* (q < 0.001, ρ > 0.5).
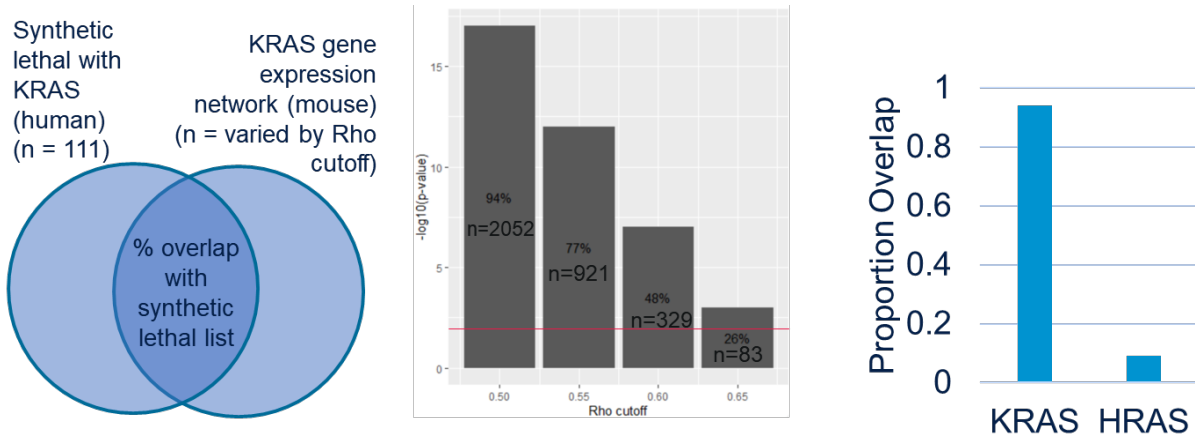
Figure 3.2 Overlap between mouse and human Ras dependencies.
Number of genes found in overlap between genes strongly correlated with Kras expression in mouse cSCCs, and genes found to be synthetic lethal with *Kras* across human cancers. As the rho cutoff changes, the overlap is depicted. The proportion overlap between genes synthetic lethal with *Kras* in human is also shown with genes strongly correlated with *Hras* expression in mouse cSCCs.
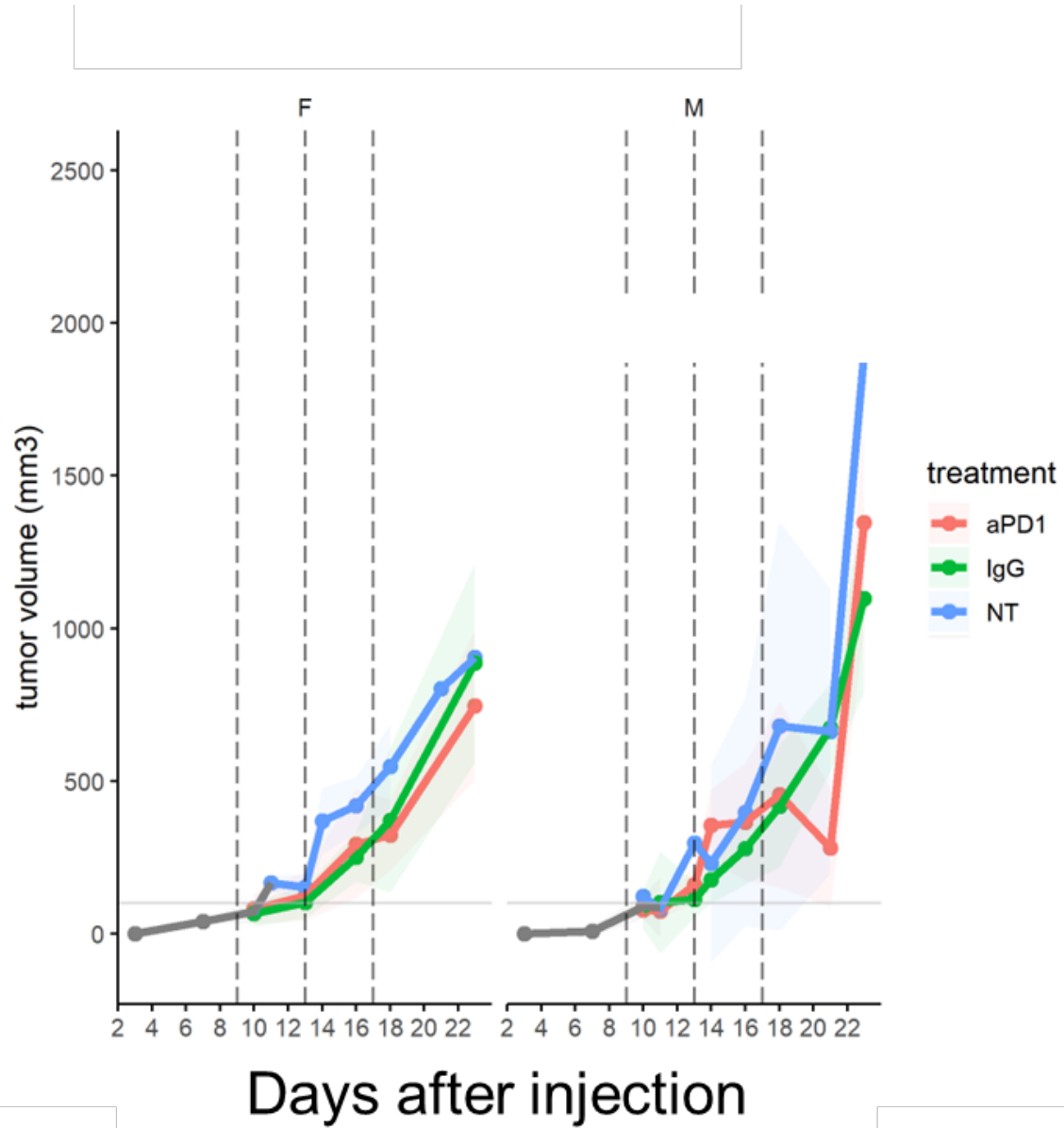
Figure 3.3 168 cells (*Kras* mutant cSCC) treated with a-PD1 in WT FVB animals. Dotted vertical lines indicate treatment day for a-PD1 or IgG. Animals are separated by male and female groups. Dots represent the average tumor volume measured within treatment group, and the shaded area represents the standard deviation.
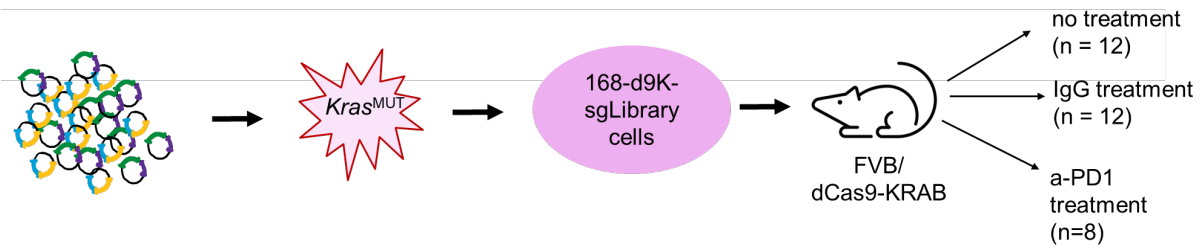
Figure 3.4 Experimental workflow for *in vivo* CRISPRi screen.
Pooled dual guide library was infected into 168 cells expressing dCas9-KRAB to generate 168-d9K-sgLibrary cells. These cells were injected into FVB/dCas9KRAB mice and the mice were randomized into 3 treatment arms as shown. Tumor volumes were monitored and mice were sacrificed 2 days following the final treatment.
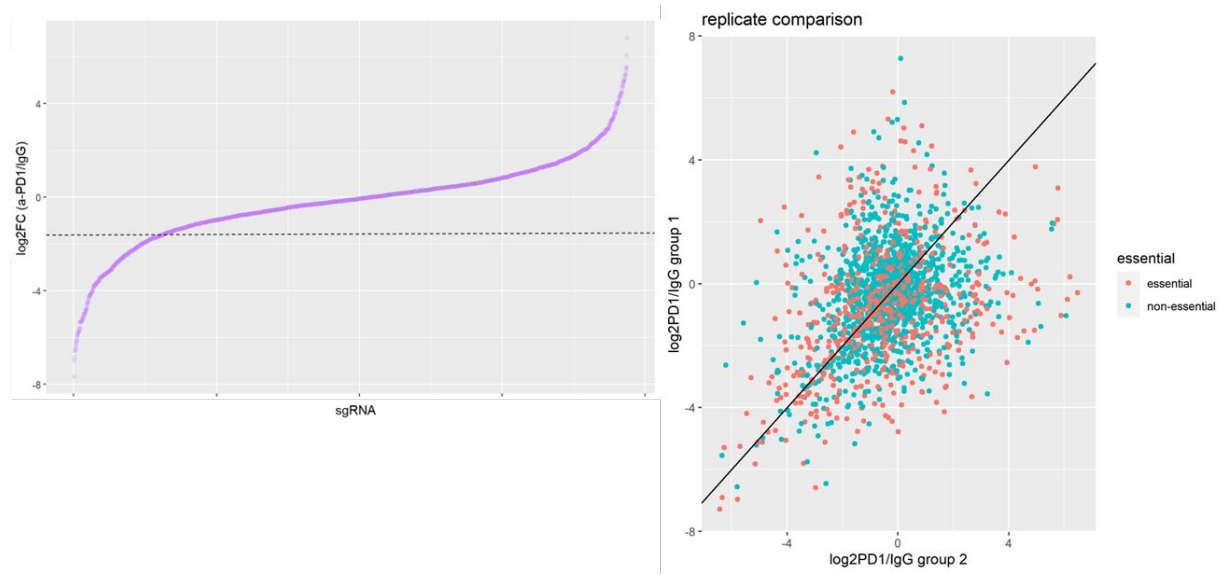
Figure 3.5 Guide performance in replicate CRISPRi screens.
a) Hits were chosen by identifying guides which dropped below the non-targeting guide effect, indicated in dotted line. b) Hits were then further streamlined by annotating genes with known essentiality for cell growth.
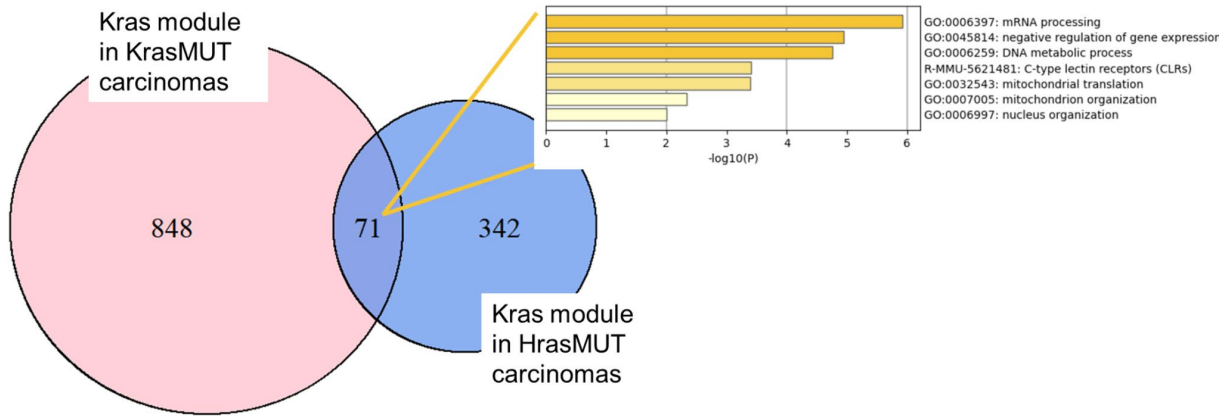
Figure 3.6 Overlap in functions enriched in coexpressed genes with *Kras* when in oncogenic and non-oncogenic status, with functions enriched in genes found as significant hits in CRISPRi screen

The genes co-expressed with *Kras* in *Kras* mutant or *Hras* mutant cSCC have conserved functions which overlap with the functions enriched in the genes identified as significant hits in the a-PD1 sensitization screen.
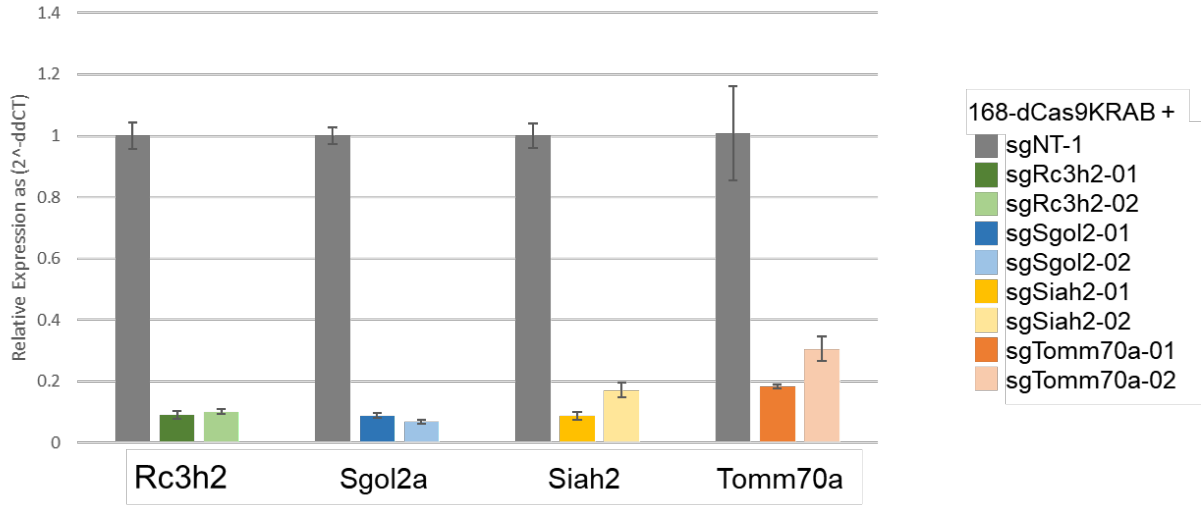
Figure 3.7 Validation cell lines for chosen screen hits demonstrate sufficient knockdown from CRISPRi dual guide construct
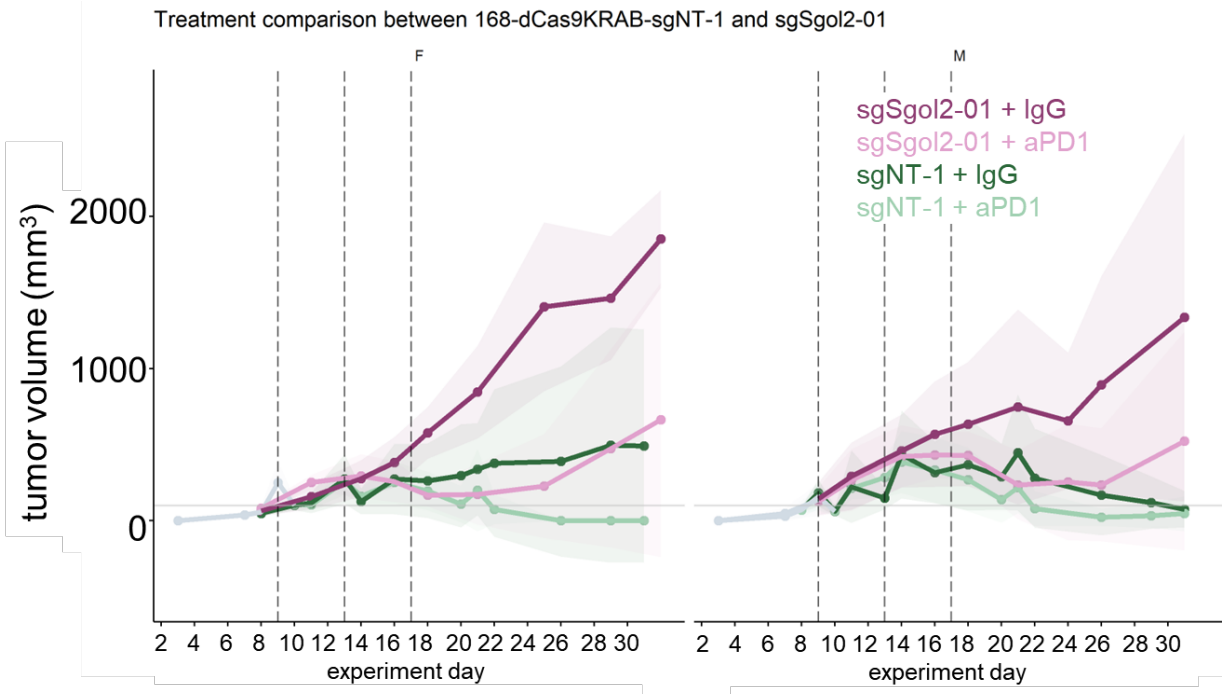
Figure 3.8 Validation experiment with hit *Sgol2* from CRISPRi screen.
168-dCas9KRAB cells expressing a dual guide for *Sgol2* or non-targeting sequence implanted in FVB/dCas9KRAB mice and treated with a-PD1 or IgG as indicated. Dotted lines indicate treatment days. Animals are separated by male and female cohorts. Dots indicate average tumor volume measured within treatment arm, and shaded area indicates standard deviation.

Figure 3.9 Waterfall plot of 168-dCas9KRAB-sgSgol2 tumors.
Change in tumor volume from first treatment day to end of experiment depicted per mouse in each treatment arm.

Figure 3.10 Waterfall plot of 168-dCas9KRAB-sgRc3h2 tumors.
Change in tumor volume from first treatment day to end of experiment depicted per mouse in each treatment arm.

Discussion

In this study, we report the design, execution, and validation of an *in vivo* CRISPRi screen for *Kras*-driven mechanisms of resistance to a-PD1 therapy. The 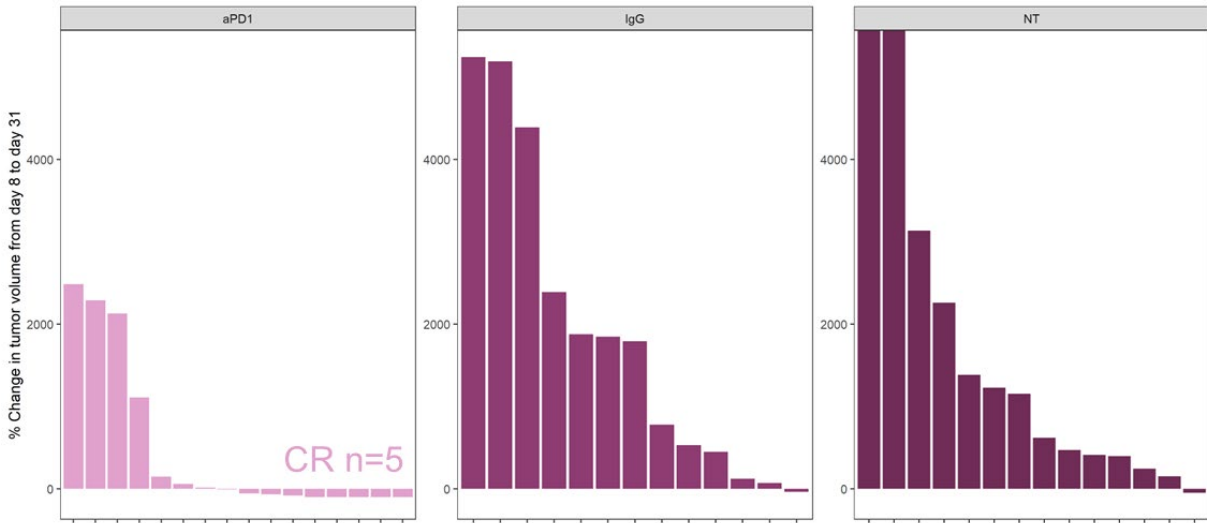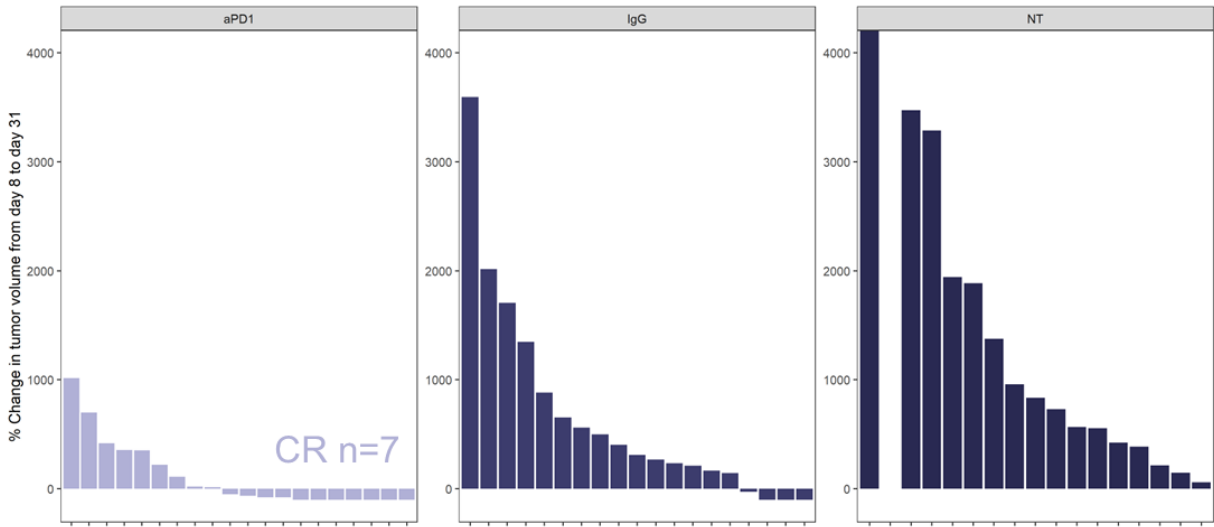growth screen and treatment *in vivo* allows us to identify clinically relevant targets which may enhance the use of a-PD1 therapy for treatment-refractory cancers. We also tested the hypothesis that gene co-expression networks contain information that is otherwise concealed by comparing replicates of two independent groups. Here, we found that the genes co-expressed with *Kras* across 67 biologically independent *Kras* mutant cSCC represented novel immunosuppressive functions, not found by differential expression analysis between *Kras* mutant and *Hras* mutant tumors.

In the process of optimizing the *in vivo* growth screen, we found that by ensuring retention of control guides we retained the power to call negative phenotype guides, or guides which dropped out. This allowed us to call a much larger group of significant hits than we expected to find. We attempted to more closely understand this group of significant hits and found that their functions overlapped with the functions shared by genes co-expressed with *Kras* in both oncogenic and normal contexts. As the oncogenic functions of *Kras* are ascribed to the constitutive activation of the *Kras* signaling, it is relevant to address the functions that are shared between the normal and oncogenic contexts. Here, we find that the immunosuppressive functions driven by *Kras* are not just oncogenic, but also found in normal functions. This role of *Kras* in providing the immune evasion that is necessary for a malignant cell to continue along transformation may prove to be critical for all tumors.

There are multiple mechanisms cancer cells can employ to evade detection by the immune system. We show that one mechanism for resensitizing 168 cells to aPD1 therapy is by increasing their PDL1 expression. The negative relationship between *Kras* expression and PDL1 expression in tumor cells may require one of the hits identified in this screen, but are yet to be

fully explored. While the aPD1 resistance mechanisms driven by *Sgol2* and *Rc3h2* are yet to be fully described, one possible explanation is related to the role of EMT phenotypes in dictating the mechanism of immune evasion present in those cells. Cutaneous SCC with mesenchymal features are more likely to express immune evasion ligands such as CD80 and CD155, while those with epithelial features express PD-L1 more strongly[38]. Thus it is possible that a consequence of *Sgol2* or *Rc3h2* activity in *Kras* mutant cSCC is to maintain a more mesenchymal phenotype[2], which is reversed in the context of losing their expression. It will be interesting to follow up on the potential to use EMT-reversing agents to resensitize a-PD1-resistant tumors to this widely approved therapy.

The demonstration here of a rational, hypothesis-driven, targeted screen approach opens the doors to more feasible *in vivo* CRISPR screens. Specifically, the validation of the significant hits from this screen, *Sgol2*, and *Rc3h2*, may also provide justification for the combinatorial treatment of a-PD1 with a sensitizing drug that will provide one more tool in the arsenal of weapons against aggressive and malignant tumors.

Materials and Methods

Gene expression networks

Bulk gene expression data were collected from 67 *Kras* mutant cutaneous squamous cell carcinomas (cSCC) from 67 independent animals treated with DMBA and TPA for 20 weeks. The Affymetrix probe for *Kras* (10549256) was correlated with all other probes across these tumors. The 1000 probes with the strongest correlation in expression with *Kras* were consolidated into genes, which resulted in 975 genes to test in our custom CRISPRi library.

CRISPRi library

The dual guide library (CRISPRi v3[27]) employs two constructs per gene, with two guides per gene. These 4 guides per gene were selected by choosing the most effective guides from a list of 10 possible sgRNAs. The library was designed with 975 genes strongly correlated to *Kras*, as described above, 25 genes with no positive correlation to *Kras*, 22 genes with known immune modulatory functions, and 30 non-targeting guides. This library was ordered from Twist Biosciences and amplified with specific PCR adapter sequences prior to cleaning with DNA Clean & Concentrator TM-5 (Cat. No.: D4013 from Zymo Research). The purified library was ligated into the pJR103BFP and pJR98 vectors at a 1:1 molar ratio.

Cell line generation

First, 168 cells (*Kras* mutant mouse cSCC cell line derived from a DMBA + TPA induced cSCC) were transfected with dCas9KRAB (pCL0029) and selected by expression of BFP by FACS (fluorescence activated cell sorting). These 168-dCas9KRAB cells were then transfected with the above described sgRNA library, selected by puromycin. To ensure adequate starting coverage of the 2000 guides in the library, the number of cells surviving puromycin selection was required to be at least 1000 cells/guide. The cells and library were sequenced to ensure the baseline representation of the intended sgRNAs.

Screen

168-dCas9KRAB-sgLibrary cells were expanded over the course of 7-14 days and collected to analyze baseline guide dropout. To achieve a starting coverage of 500x across the 2000 sgRNAs we screened, we injected 1e6 cells into the right subcutaneous mouse flank. All animal experiments were approved by the Institutional Animal Care and Use Committee (IACUC) of the University of California, San Francisco (UCSF) and performed under the approved protocol. For all experiments, equal numbers of male and female 7-9 week old FVB/dCas9KRAB animals were

used. FVB/dCas9KRAB mice were a generous gift from Dr. Michael McManus at UCSF. All animals were housed in standard conditions, with standard 12 hour light cycle, and monitored for pathogen and injury-free conditions. Approximately one week after injection, mice were randomized by tumor size into treatment groups to account for consistent average starting tumor sizes at the start of the experiment. Where possible, treatment groups were randomized to minimize cage effect and age. All experiments were randomized within gender, in order to later assess within and between gender effects.

Treatments + tissue collection

Mice were weighed on randomization day, and the average weight within males or females was used to dilute a dose of 0.1 mg/kg antibody in sterile PBS from the stock antibody. The mouse a-PD1 and control IgG were generous gifts from Bristol Myers Squibb. Treatments were given by intraperitoneal injection 3 times, 4 days apart. Tumors were measured by digital calipers every 2-3 days to monitor growth rates. All cohorts of the experiment were terminated on the second day after the final treatment to collect enough tumor for downstream analysis.

Genomic DNA extraction

Tumors were chopped and digested for genomic DNA extraction following manufacturer protocols (Macherey Nagel Ref.740950.50). All available DNA was PCR amplified then purified for sgRNA sequences by target capture amplification. Illumina sequencing adapters were ligated and the libraries were sequenced on Illumina NovaSeq X (Sequencing was performed at the UCSF CAT, supported by UCSF PBBR, RRP IMIA, and NIH 1S10OD028511-01 grants).

Alignment and analysis of sgRNA sequencing

Custom alignment pipelines were built based on the methods included in Replogle et al.[27]. Requests for materials and methods, or any questions, can be directed to

bollamsaumya@gmail.com or allan.balmain@ucsf.edu. Briefly, the expected guide library was used as the template to align the dual guide sequences found in each sample. A successfully counted read aligned to a specific gene was required to contain 1) both correct guides in any orientation and 2) no mismatched bases. These counts were then used to assess the library representation within each sample and the expected read counts from the non-targeting guides. For each guide, the log2FC was calculated between the a-PD1 treated arm and IgG treated arm. First, 0 counts were replaced for guides which had no successfully aligned reads. The average reads per million (RPM) in each arm was normalized with the total successfully aligned reads in each sample. To compare the guide representation in the a-PD1 treated arm compared with IgG, or IgG with the non-treated arm, the log2foldchange (log2FC) of the average RPM +1 was calculated for each group.

Hit validation experiments

Individual gene knockdown cell lines were generated as described above, by transfecting 168-dCas9KRAB cells with the guide construct of interest. For the screen hits being validated, the same guide sequences used in the library were individually transfected as each dual guide construct and selected with puromycin. To confirm the knockdown efficiency, RNA was isolated from the stably cultured cell line and expression of the knockdown gene was compared to expression of Gapdh, using a control cell line expressing one non-targeting guide. The $2^{\wedge}\text{-ddCT}$ is reported. *In vivo* treatment experiments were conducted by injecting 1e5 cells into the right subcutaneous flank of FVB/dCas9KRAB mice. Again, mice were weighed and randomized into treatment arms (a-PD1, IgG, no treatment) when the average tumor volume reached 100mm^3 across all mice in the cohort. Mice were treated with an intraperitoneal (IP) injection of 0.1 mg/kg antibody in sterile PBS 3 times, 4 days apart. Tumor volumes were measured with digital calipers every 2-3 days to monitor tumor growth in each arm for a total of 31 days.

Chapter 4: Conclusions and future directions

The body of work described here details the roles of *Hras* and *Kras* in either normal or oncogenic contexts as they relate to tumor-immune interactions during multiple stages of tumor evolution. Considerations of the normal functions of human oncogenes must accompany those of the transformed context to achieve a complete understanding of tumor progression. Malignant cells exist in the context of a complex microenvironment, first as the minority population latently present in a pathologically normal tissue, and then as a self-sufficient population of cells which outcompete the host organ. Across these stages, the immunological response to these cells must be carefully controlled. Importantly, understanding these responses across different phases of tumor evolution could lend crucial insights to the advancement of both early detection of cancer and enhanced therapeutic protocols for advanced disease.

In Chapter 2, I describe the wild-type roles of *Hras* and *Kras* in responding to tumor-promoting inflammation. Here, we demonstrated that *Hras* is required for TPA-induced keratinization processes that resemble a wound-healing environment. The *Hras*^MUT carcinomas resulting from DMBA and TPA exposure reflect the consequences of hyperactivated epidermal processes, as this readily produces papillomas and carcinomas. We also demonstrate an *Hras*-dependent axis for regulatory T cell recruitment, whereby immune surveillance for mutant cells might be balanced, permitting the survival and progression of neoplastic cells. Given that fewer papillomas arise in the absence of *Hras*, this suggests that *Kras*-driven signals alone may not be sufficient to facilitate TPA-induced promotion. Even so, *Kras*-driven induction of proliferation and inflammation can lead to papillomas with the added functions of mutant *Kras*.

The stark tissue tropism of *Hras* and *Kras* driven human cancers remains an unanswered question. What endogenous, tissue-specific, processes may be leading to *Kras* mutant pancreatic adenocarcinomas, rather than *Hras*? Future work will expand on the findings described here to help understand questions like these. Additionally, the normal role of *Kras* is described here in the unnatural context of a germline *Hras* knockout. It would be interesting to follow up on these findings by addressing the inflammatory promotion mechanisms driven by *Kras* in the wildtype setting. This would be useful to address in the context of tissue known to develop *Kras* mutant tumors. Here, we could then clearly define the cooperative role of *Hras* in the context of *Kras*-dependent tumorigenesis.

Nevertheless, this work sets the stage for an important line of future contributions to the understanding of the first steps of tumorigenesis. As the importance of non-mutagenic, promoting, processes become more and more visible, the relationship between these mechanisms and the driving oncogenes is of vital importance. I look forward to following how this field evolves and adjusts its theories to explain this incredibly complex process of tumorigenesis.

In Chapter 3, I describe the role of mutant *Kras* in allowing carcinomas to evade immune detection. Here, we demonstrated the ability to perform an *in vivo* CRISPRi screen with a syngeneic model, that reliably captured negative phenotype hits. This allowed me to identify genes correlated with oncogenic *Kras* which conferred resistance to a-PD1 therapy by reducing PD-L1 expression. *Sgol2* and *Rc3h2* may thus present novel opportunities for combination therapy with a-PD1, as sensitizing *Kras* mutant tumors to a-PD1 therapy would provide much needed improvement in available therapeutic options.

At the outset of this project, there had not been any reported studies of *in vivo* CRISPR screens of any kind (CRISPR, CRISPRi, etc). We conducted a thorough set of optimization and

control experiments to demonstrate the reliability of our results from an *in vivo* growth screen. We have been encouraged by the emerging reports from other groups successfully conducting similar screens, and are eagerly following the space to understand possible optimizations. Yet, this experiment still relied on the *in vitro* transfection and generation of the guide library expressing cell line, before transplanting the cell line into the mouse model. The challenges associated with *in vivo* transfection, i.e. delivery of sgRNA libraries, are numerous and specific for each tissue in question, but is the necessary next step to a screen like this. Indeed, the first reports of such studies are beginning to emerge, demonstrating the feasibility of a fully *in vivo* conducted CRISPR screen[39].

While it is compelling to conduct genome-wide screens where the technical considerations allow it, the appeal of a hypothesis-driven, targeted, screen is that the signal-to-noise is far greater. With the consideration of advancing therapeutic options for the sickest patients, it is compelling to consider the most optimal experimental strategies whose results will be recapitulated in translational experiments. In the upcoming studies, I hope to continue finding evidence for the combinatorial strategy of a-PD1 with targeting of *Rc3h2* or *Sgol2*, as well as mechanistic explanations for this therapy design.

The results described in this dissertation represent not only the commitment to answering difficult questions, but also the belief that we can build methods to answer previously unanswerable questions. As we continue to face these questions of fundamental biology, I look forward to being surprised, awed, and challenged by the marvelous complexities of cancer biology.

References

1. Coussens, L. M. & Werb, Z. Inflammation and cancer. *Nature* **420**, 860–867 (2002).

2. Wong, C. E. *et al.* Inflammation and *Hras* signaling control epithelial-mesenchymal transition during skin tumor progression. *Genes Dev.* **27**, 670–682 (2013).

3. Martincorena, I. *et al.* Somatic mutant clones colonize the human esophagus with age. *Science* **362**, 911–917 (2018).

4. Martincorena, I. *et al.* Tumor evolution. High burden and pervasive positive selection of somatic mutations in normal human skin. *Science* **348**, 880–886 (2015).

5. Zafra, M. P. *et al.* An Allelic Series Reveals Distinct Phenotypes of Common Oncogenic Variants. *Cancer Discov.* **10**, 1654–1671 (2020).

6. Ninomiya, Y. *et al.* K-Ras and H-Ras activation promote distinct consequences on endometrial cell survival. *Cancer Res.* **64**, 2759–2765 (2004).

7. Walsh, A. B. & Bar-Sagi, D. Differential activation of the Rac pathway by Ha-Ras and K-Ras. *J. Biol. Chem.* **276**, 15609–15615 (2001).

8. Najumudeen, A. K. *et al. KRAS* allelic imbalance drives tumour initiation yet suppresses metastasis in colorectal cancer *in vivo*. *Nat. Commun.* **15**, 100 (2024).

9. Zhang, Z. *et al.* Wildtype *Kras*2 can inhibit lung carcinogenesis in mice. *Nat. Genet.* **29**, 25–33 (2001).

10. Kong, G. *et al.* Loss of wild-type *Kras* promotes activation of all Ras isoforms in oncogenic *Kras*-induced leukemogenesis. *Leukemia* **30**, 1542–1551 (2016).

11. Xu, J. *et al.* Dominant role of oncogene dosage and absence of tumor suppressor activity in Nras-driven hematopoietic transformation. *Cancer Discov.* **3**, 993–1001 (2013).

12. Gallini, S. *et al.* Injury prevents Ras mutant cell expansion in mosaic skin. *Nature* **619**, 167–175 (2023).

13. McCreery, M. Q. *et al.* Evolution of metastasis revealed by mutational landscapes of

chemically induced skin cancers. *Nat. Med.* **21**, 1514–1520 (2015).

14. Dimon, M. T. *et al.* No evidence for integrated viral DNA in the genome sequence of cutaneous squamous cell carcinoma. *J. Invest. Dermatol.* **134**, 2055–2057 (2014).

15. Bremner, R., Kemp, C. J. & Balmain, A. Induction of different genetic changes by different classes of chemical carcinogens during progression of mouse skin tumors. *Mol. Carcinog.* **11**, 90–97 (1994).

16. Casar, B. *et al.* RAS at the Golgi antagonizes malignant transformation through PTPRκ-mediated inhibition of ERK activation. *Nat. Commun.* **9**, 3595 (2018).

17. Chiu, V. K. *et al.* Ras signalling on the endoplasmic reticulum and the Golgi. *Nat. Cell Biol.* **4**, 343–350 (2002).

18. Quigley, D. A. *et al.* Gene Expression Architecture of Mouse Dorsal and Tail Skin Reveals Functional Differences in Inflammation and Cancer. *Cell Rep.* **16**, 1153–1165 (2016).

19. Schlingemann, J. *et al.* Profile of gene expression induced by the tumour promotor TPA in murine epithelial cells. *Int. J. Cancer* **104**, 699–708 (2003).

20. Sandoval, M., Ying, Z. & Beronja, S. Interplay of opposing fate choices stalls oncogenic growth in murine skin epithelium. *Elife* **10**, (2021).

21. Pineda, C. M. *et al.* Hair follicle regeneration suppresses Ras-driven oncogenic growth. *J. Cell Biol.* **218**, 3212–3222 (2019).

22. Newman, A. M. *et al.* Robust enumeration of cell subsets from tissue expression profiles. *Nat. Methods* **12**, 453–457 (2015).

23. Hill, W. *et al.* Lung adenocarcinoma promotion by air pollutants. *Nature* **616**, 159–167 (2023).

24. Wang, F. *et al.* Regulation of epithelial transitional states in murine and human pulmonary fibrosis. *J Clin Invest* **133**, (2023).

25. Schupp, P. G. *et al.* Deconstructing Intratumoral Heterogeneity through Multiomic and Multiscale Analysis of Serial Sections. *Cancers* **16**, (2024).

26. Horlbeck, M. A. *et al.* Compact and highly active next-generation libraries for CRISPR-mediated gene repression and activation. *Elife* **5**, (2016).

27. Replogle, J. M. *et al.* Maximizing CRISPRi efficacy and accessibility with dual-sgRNA libraries and optimal effectors. *Elife* **11**, (2022).

28. Huang, Q. *et al.* Loss of sensitizes immune checkpoint blockade in non-small cell lung cancer. *Sci Adv* **8**, eabi9533 (2022).

29. Li, F. *et al.* Epigenetic CRISPR Screen Identifies as an Immunotherapeutic Target in -Mutant Lung Adenocarcinoma. *Cancer Discov.* **10**, 270–287 (2020).

30. Wang, X. *et al. In vivo* CRISPR screens identify the E3 ligase Cop1 as a modulator of macrophage infiltration and cancer immunotherapy target. *Cell* **184**, 5357–5374.e22 (2021).

31. Guirguis, A. A. *et al.* Inhibition of METTL3 Results in a Cell-Intrinsic Interferon Response That Enhances Antitumor Immunity. *Cancer Discov.* **13**, 2228–2247 (2023).

32. Dodagatta-Marri, E. *et al.* α-PD-1 therapy elevates Treg/Th balance and increases tumor cell pSmad3 that are both targeted by α-TGFβ antibody to promote durable rejection and immunity in squamous cell carcinomas. *J Immunother Cancer* **7**, 62 (2019).

33. Hu, Q., Liu, Q., Zhao, Y., Zhang, L. & Li, L. SGOL2 is a novel prognostic marker and fosters disease progression via a MAD2-mediated pathway in hepatocellular carcinoma. *Biomark. Res.* **10**, 82 (2022).

34. Tian, X. *et al.* Identification of tumor-infiltrating immune cells and prognostic validation of tumor-infiltrating mast cells in adrenocortical carcinoma: results from bioinformatics and real-world data. *Oncoimmunology* **9**, 1784529 (2020).

35. Vogel, K. U. *et al.* Roquin paralogs 1 and 2 redundantly repress the Icos and Ox40 costimulator mRNAs and control follicular helper T cell differentiation. *Immunity* **38**, 655–668 (2013).

36. Zhou, M. *et al.* Roquin2 suppresses breast cancer progression by inhibiting tumor angiogenesis via selectively destabilizing proangiogenic factors mRNA. *Int. J. Biol. Sci.* **17**,

2884–2898 (2021).

37. Choi, J., Saraf, A., Florens, L., Washburn, M. P. & Busino, L. PTPN14 regulates Roquin2 stability by tyrosine dephosphorylation. *Cell Cycle* **17**, 2243–2255 (2018).

38. Lorenzo-Sanz, L. *et al.* Cancer cell plasticity defines response to immunotherapy in cutaneous squamous cell carcinoma. *Nat. Commun.* **15**, 5352 (2024).

39. Liu, S. J. *et al. In vivo* perturb-seq of cancer and microenvironment cells dissects oncologic drivers and radiotherapy responses in glioblastoma. *Genome Biol* **25**, 256 (2024).

Publishing Agreement

It is the policy of the University to encourage open access and broad distribution of all theses, dissertations, and manuscripts. The Graduate Division will facilitate the distribution of UCSF theses, dissertations, and manuscripts to the UCSF Library for open access and distribution. UCSF will make such theses, dissertations, and manuscripts accessible to the public and will take reasonable steps to preserve these works in perpetuity.

I hereby grant the non-exclusive, perpetual right to The Regents of the University of California to reproduce, publicly display, distribute, preserve, and publish copies of my thesis, dissertation, or manuscript in any form or media, now existing or later derived, including access online for teaching, research, and public service purposes.

Author Signature

10/29/2024

Date